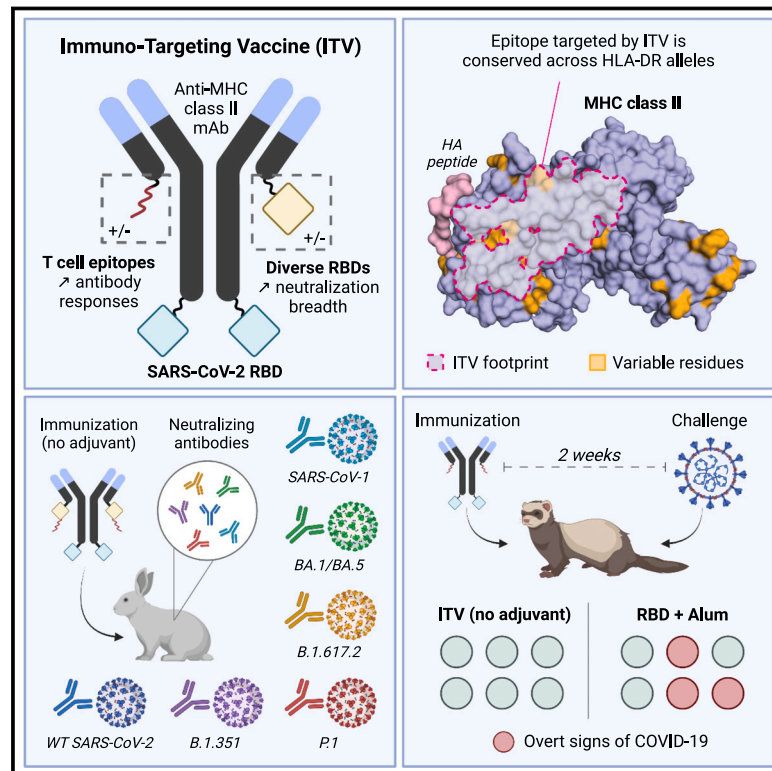


Modular adjuvant-free pan-HLA-DR-immunotargeting subunit vaccine against SARS-CoV-2 elicits broad sarbecovirus-neutralizing antibody responses

Graphical abstract



Authors

Audrey Kassardjian, Eric Sun, Jamie Sookhoo, ..., Shawn Babiuk, Brian Barber, Jean-Philippe Julien

Correspondence

jean-philippe.julien@sickkids.ca

In brief

Kassardjian et al. engineer and characterize a modular vaccine scaffold for the delivery of antigen to MHC class II on antigen-presenting cells. This protein vaccine induces broad sarbecovirus neutralizing antibody responses and protects from SARS-CoV-2 viral challenge independently of adjuvant co-administration.

Highlights

- Modular ITV design consists of SARS-CoV-2 spike RBD fused to a pan-MHC class II mAb
- Structure of conserved epitope on HLA-DR offers molecular basis of broad reactivity
- Adjuvant-free ITV immunization elicits broad neutralizing Ab responses in rabbits
- Adjuvant-free ITV immunization protects ferrets from SARS-CoV-2 challenge



Article

Modular adjuvant-free pan-HLA-DR-immunotargeting subunit vaccine against SARS-CoV-2 elicits broad sarbecovirus-neutralizing antibody responses

Audrey Kassardjian,^{1,2} Eric Sun,^{1,2} Jamie Sookhoo,^{3,4} Krithika Muthuraman,^{1,5} Kayluz Frias Boligan,⁶ Iga Kucharska,¹ Edurne Rujas,^{1,7,8,9} Arif Jetha,¹ Donald R. Branch,^{6,10} Shawn Babiuk,^{3,4} Brian Barber,² and Jean-Philippe Julien^{1,2,5,11,*}

¹Program in Molecular Medicine, The Hospital for Sick Children Research Institute, Toronto, ON M5G 0A4, Canada

²Department of Immunology, University of Toronto, Toronto, ON M5S 1A8, Canada

³Canadian Food Inspection Agency, National Centre for Foreign Animal Disease, Winnipeg, MB R3E 3M4, Canada

⁴Department of Immunology, University of Manitoba, Winnipeg, MB R3E 0T5, Canada

⁵Department of Biochemistry, University of Toronto, Toronto, ON M5S 1A8, Canada

⁶Canadian Blood Services, Keenan Research Centre, Toronto, ON M5B 1W8, Canada

⁷Ikerbasque, Basque Foundation for Science, 48013 Bilbao, Spain

⁸Pharmacokinetic, Nanotechnology and Gene Therapy Group, Faculty of Pharmacy, University of the Basque Country UPV/EHU, 01006 Vitoria, Spain

⁹Bioaraba, Microbiology, Infectious Disease, Antimicrobial Agents, and Gene Therapy, 01006 Vitoria, Spain

¹⁰University of Toronto, Departments of Medicine and Laboratory Medicine and Pathobiology, Toronto, ON M5S 1A8, Canada

¹¹Lead contact

*Correspondence: jean-philippe.julien@sickkids.ca

<https://doi.org/10.1016/j.celrep.2023.112391>

SUMMARY

Subunit vaccines typically require co-administration with an adjuvant to elicit protective immunity, adding development hurdles that can impede rapid pandemic responses. To circumvent the need for adjuvant in a severe acute respiratory syndrome coronavirus 2 (SARS-CoV-2) subunit vaccine, we engineer a thermo-stable immunotargeting vaccine (ITV) that leverages the pan-HLA-DR monoclonal antibody 44H10 to deliver the viral spike protein receptor-binding domain (RBD) to antigen-presenting cells. X-ray crystallography shows that 44H10 binds to a conserved epitope on HLA-DR, providing the basis for its broad HLA-DR reactivity. Adjuvant-free ITV immunization in rabbits and ferrets induces robust anti-RBD antibody responses that neutralize SARS-CoV-2 variants of concern and protect recipients from SARS-CoV-2 challenge. We demonstrate that the modular nature of the ITV scaffold with respect to helper T cell epitopes and diverse RBD antigens facilitates broad sarbecovirus neutralization. Our findings support anti-HLA-DR immunotargeting as an effective means to induce strong antibody responses to subunit antigens without requiring an adjuvant.

INTRODUCTION

Since the emergence of severe acute respiratory syndrome coronavirus 2 (SARS-CoV-2) in December of 2019, joint efforts by the global scientific community have led to the development and deployment of vaccines at an unprecedented rate.^{1,2} Currently licensed vaccines against SARS-CoV-2 have countered the advance of the pandemic with considerable success; however, disparities in global vaccination coverage, persistence of circulating virus, and continued viral evolution have highlighted a need to address the limitations of existing vaccine approaches. Against pandemic pathogens, vaccines must exhibit high efficacy and ideally provide durable immunity and broad protection against continuously emerging variants of concern (VOCs). Moreover, vaccines with favorable profiles for manufacturing and distribution would enable their deployment in countries with limited infrastructure for storage and distribution, thereby increasing vaccine accessibility in future pandemic settings.^{3,4}

Recombinant protein subunit vaccines can provide safe and effective vaccination options for use across diverse populations. Against rapidly changing pathogens, subunit-based approaches offer numerous developmental efficiencies that can be leveraged for pandemic responses, including rapid scalability, low development and distribution costs, and a reduced reliance on sophisticated cold-chain infrastructure. However, due to the limited intrinsic immunogenicity of purified protein antigens, subunit vaccine formulations usually require immunostimulatory agents to enhance the immune response.⁵ The diversity of available adjuvants, each with distinct modes of action, coupled with the unique nature of each antigen-adjuvant pairing, poses considerable development challenges for the time-sensitive deployment of adjuvanted subunit vaccines.^{6,7} Moreover, constraints imposed by the global supply and availability of widely used adjuvants have further precluded the efficient development of subunit vaccines for large-scale manufacturing.^{8–10} To this end, alternative strategies for increasing vaccine immunogenicity without requisite



pairing of protein immunogens to extrinsic adjuvant systems remain a central pursuit in vaccine research.

Targeted antigen delivery, also known as immunotargeting, is one such strategy proposed to facilitate antigen uptake, processing, and presentation by antigen-presenting cells (APCs), thereby enhancing vaccine-induced immune activation. Previous studies have demonstrated the success of targeting APC receptors (such as major histocompatibility complex [MHC] class II, C-type lectin-like receptors, and tumor necrosis factor [TNF] receptor family members) in enhancing immune responses to various recombinant antigens following vaccination.^{11–14} One particular MHC class II-targeting monoclonal antibody (mAb), 44H10, has been successfully used in an immunotargeting context to elicit antigen-specific antibody responses for multiple vaccine candidates,^{15–19} even in the absence of adjuvant. Though 44H10 was first discovered as an anti-HLA-DR antibody, it is also cross-reactive with rabbit and ferret MHC class II molecules,^{16,20,21} enabling the *in vivo* characterization of MHC class II-targeting vaccine candidates in these pre-clinical species. Providing a source of efficient helper T cell activation is another independent strategy for enhancing vaccine immunogenicity. Inclusion of universal helper T cell epitopes can allow binding to MHC class II molecules irrespective of population-level allelic variation to provide effective T cell help necessary for optimal antibody responses.^{22–25}

In this work, we report the engineering, structural characterization, and pre-clinical evaluation of a thermostable adjuvant-free SARS-CoV-2 vaccine candidate that leverages the MHC class II-targeting properties of mAb 44H10 to elicit protective neutralizing antibody responses against the SARS-CoV-2 receptor-binding domain (RBD). We furthermore explore the role of synthetic and naturally derived T cell epitopes in enhancing vaccine immunogenicity. Lastly, we describe the modular nature of the immunotargeting vaccine (ITV) immunoglobulin scaffold that enables the incorporation of RBDs from multiple sarbecoviruses on a single vaccine candidate to broaden the elicited neutralizing response.

RESULTS

ITV effectively targets SARS-CoV-2 RBD antigen to MHC class II

To engineer an ITV with desirable biochemical and immunological properties, we fused the SARS-CoV-2 RBD to the heavy chain C terminus of a chimeric 44H10 antibody (c44H10) with mouse variable and human constant regions (Figure 1A). SDS-PAGE analysis of purified soluble RBD, c44H10 immunoglobulin G (IgG), and ITV demonstrated the expected increase in the overall size of the recombinantly expressed ITV relative to c44H10 IgG under both non-reducing and reducing conditions (Figure 1B). Indeed, an upward shift of the c44H10 heavy-chain band by ~25 kDa in the ITV was observed, corresponding to the RBD linkage to the ITV heavy chain. The hydrodynamic radius of the ITV (9 nm) roughly corresponded to the sum of radii measured for RBD and c44H10 (3.3 and 5.9 nm, respectively) (Figure 1C). Visualization of purified ITV by negative-stain electron microscopy further confirmed the incorporation of two RBDs per ITV molecule, with considerable flexibility between

the c44H10 IgG scaffold and RBDs as conferred by the 10-amino acid polypeptide linker joining these domains (Figures 1D and S1).

ITV was found to bind MHC class II on the human B lymphoblastoid cell line BJAB in flow cytometry experiments (Figure 1E), and the strength of this interaction was measured by biolayer interferometry (BLI) using recombinant HLA-DR, with an apparent K_D of 1.5 nM (Figure 1F). In addition, the structural integrity of the RBD antigen in the context of the ITV was confirmed by flow cytometry using a panel of four mAbs targeting distinct conformational epitopes on the SARS-CoV-2 RBD (class I to IV)^{26–31} (Figure 1G). Together, these data demonstrate the ability of the ITV to incorporate the intended biophysical and functional properties of its constituents, retaining both the structural integrity of the RBD antigen and the MHC class II-targeting ability of the 44H10 antibody.

c44H10 binds a conserved site on HLA-DR

A desirable characteristic of any vaccine is its ability to function effectively across the entire target population. As one of the most polymorphic set of alleles,³² targeting to MHC class II represents a considerable challenge, and an effective ITV targeting HLA-DR would need to overcome the vast majority of—if not all—HLA-DR allelic variation present within the human population. To evaluate the robustness of the 44H10 antibody against HLA-DR allelic variation, the binding of c44H10 was tested against a random set of 100 different donor peripheral blood mononuclear cell (PBMC) samples from the Greater Toronto Area. The c44H10 antibody was reactive against 100% of the samples tested (Figure 2A), suggesting broad reactivity of the 44H10 specificity toward HLA-DR allelic variants in humans.

To determine the extent to which 44H10 targets a truly monomorphic epitope on HLA-DR, as suggested by previous literature describing reactivity to *DR-1*, *-2*, *-3*, *-4*, *-5*, and *-7* phenotypes,²⁰ we solved the crystal structure of the c44H10 Fab in complex with the extracellular HLA-DR α/β heterodimer (HLA-DRA*01:01, HLA-DRB1*04:01) by X-ray crystallography at a resolution of 3.1 Å (Figure 2B; Table S1). Structural analysis of the co-complex revealed that c44H10 binds away from the HLA-DR peptide-binding groove, avoiding regions of concentrated diversity (Figures 2B and S2A). Instead, antibody-HLA-DR interactions are predominantly mediated by the practically invariable HLA-DR α chain, which contributes over 70% of the interface buried surface area (BSA) (α chain BSA = 742 Å²; total BSA = 1,066 Å²) and mediates 10 of the 13 intermolecular hydrogen bonds (Figure 2C; Tables S2 and S3). Sequence alignment to the IPD-MHC database indicated that most HLA-DR residues contacted by c44H10 are conserved across major -DRA and -DRB1 allele groups. Only three residues at the outmost periphery of the antibody-HLA interface (contributing only ~0.4% of the interface total BSA) displayed slight sequence variability in other HLA-DR allele groups, namely α -W168, β -F58, and β -H60 (Figures 2C and S2A–S2C). We assessed the impact of this variability on c44H10 antibody binding by generating a panel of recombinant HLA-DR mutants substituting these residues with their counterparts from other HLA-DR alleles. BLI studies revealed that substitutions at these three positions minimally hindered the ability of c44H10 to bind HLA-DR (Figure 1D). Thus,

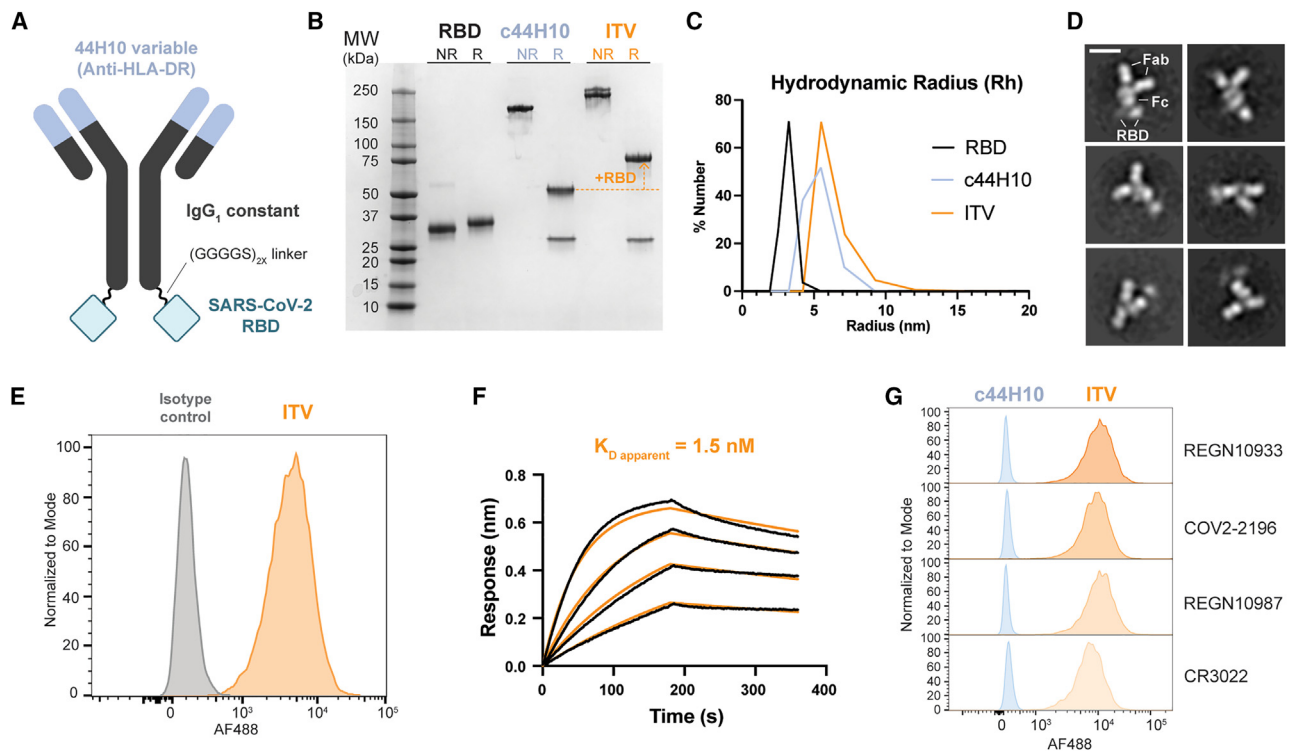


Figure 1. Biophysical and functional characterization of the ITV against SARS-CoV-2

(A) Schematic representation of the ITV against SARS-CoV-2 created with BioRender.com.
 (B) SDS-PAGE of purified RBD, c44H10 IgG, and ITV under non-reducing (NR) and reducing (R) conditions.
 (C) Dynamic light scattering profiles of RBD, c44H10 IgG, and ITV.
 (D) Representative 2D class averages from negative-stain electron microscopy images of purified ITV. The white scale bar on the top left panel corresponds to 10 nm. See also Figure S1.
 (E) Flow cytometric detection of ITV binding to MHC class II expressed on BJAB cells.
 (F) Biolayer interferometry binding profile of purified ITV to recombinant HLA-DR, where black lines represent measured binding and orange curves correspond to the data fitted to a 1:1 binding model ($R^2 = 0.99$).
 (G) Binding of class I (REGN10933), II (COV2-2196), III (REGN10987), and IV (CR3022) mAbs targeting distinct RBD conformational epitopes to ITV measured by flow cytometry.

the structural characterization of the c44H10-HLA-DR interaction in the context of comprehensive MHC class II genetic sequence databases demonstrates the ability of the ITV to overcome extreme HLA-DR polymorphisms in the human population by binding to a conserved epitope.

Unadjuvanted ITV immunization elicits robust neutralizing antibody responses in rabbits

To evaluate the immunogenicity of the ITV and assess the benefit of immunotargeting, rabbits were immunized subcutaneously (s.c.) in a prime-boost regimen with either 50 μ g unadjuvanted ITV or an equimolar dose of soluble RBD (sRBD) (Figure 3A). While unadjuvanted sRBD immunization did not elicit significant antibody responses, ITV immunization induced robust anti-RBD IgG titers, particularly after a booster dose at day 35 post-priming (Figure 3B). Initial assessment of the functional quality of the elicited antibody response from ITV-immunized rabbits was carried out using an ELISA-based surrogate virus neutralization (sVNT) assay, which evaluates the ability of serum antibodies to disrupt the RBD-ACE2 interaction.^{36,37}

ITV immunization elicited RBD-neutralizing antibody responses that peaked after the boost (day 49; $ED_{50} = 0.0064$) and persisted over the experimental time frame (Figure 3C). These data were corroborated by an orthogonal pseudovirus neutralization (pVNT) assay (Figure 3D), which measures the ability of serum antibodies to block the infection of 293T cells expressing the human ACE2 (hACE2) receptor by SARS-CoV-2 spike-pseudotyped lentivirus.³⁸ Relative to the sVNT, the pVNT assay offers increased sensitivity through the detection of antibodies that neutralize via mechanisms other than steric hindrance or occlusion of the ACE2 binding site.^{27,39} Neutralization titers derived from both assays were not significantly different (Figure 3E), suggesting that the neutralizing antibody response elicited by the ITV was largely driven by steric hindrance or occlusion of the ACE2 binding site, as would be expected from an RBD-based immunogen. In contrast, no neutralization in the sera of rabbits immunized with sRBD was detected by either method. Collectively, these data demonstrate the ability of unadjuvanted ITV to elicit neutralizing antibody responses in immunized rabbits.

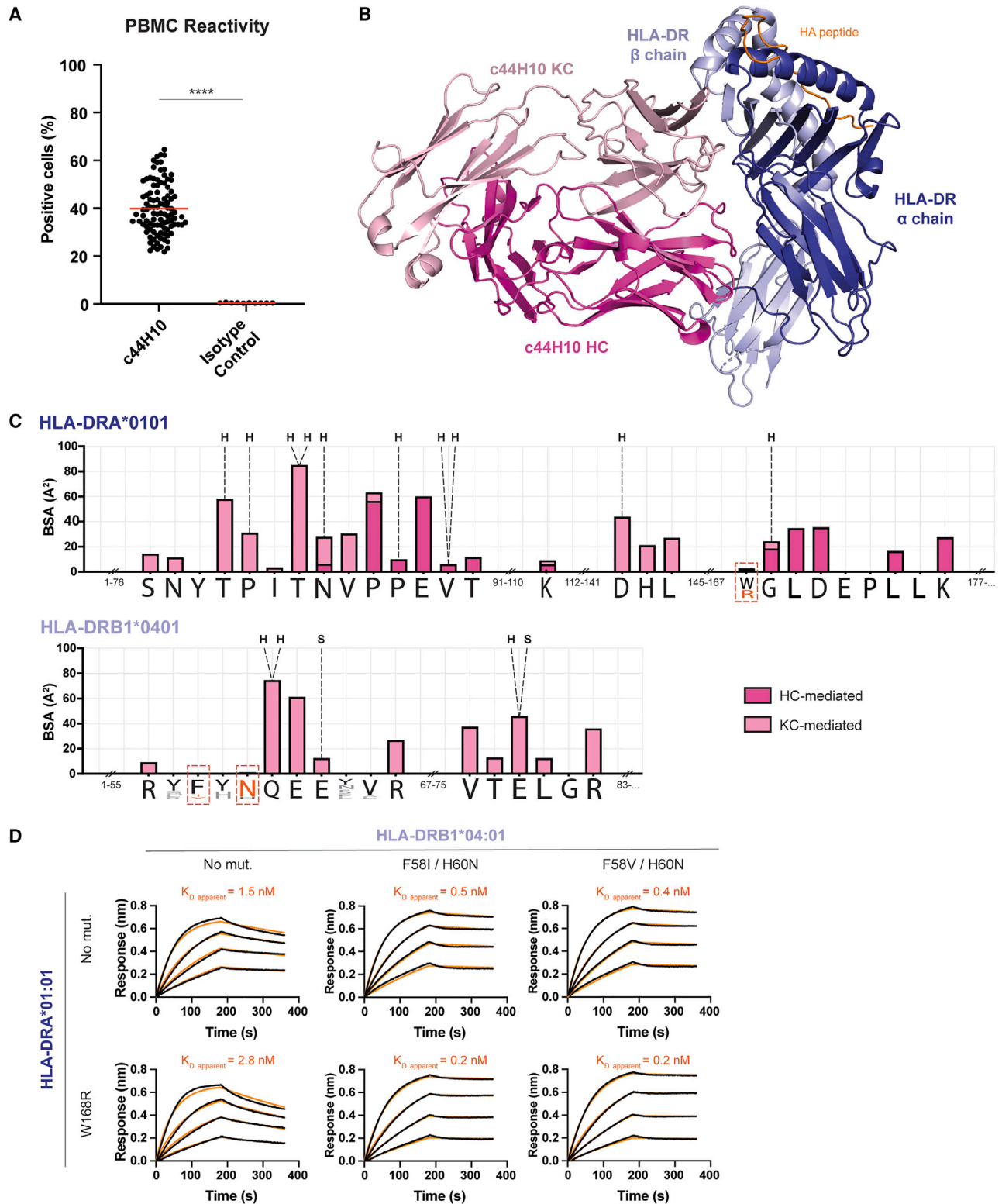


Figure 2. Molecular basis of MHC class II targeting by c44H10

(A) Flow cytometric detection of c44H10 IgG binding to 100 donor PBMC samples from the Greater Toronto Area. Data are represented as reactivity to individual PBMC samples + mean reactivity in each group (marked by the red lines) and analyzed by unpaired t test (**** $p < 0.0001$).

(legend continued on next page)

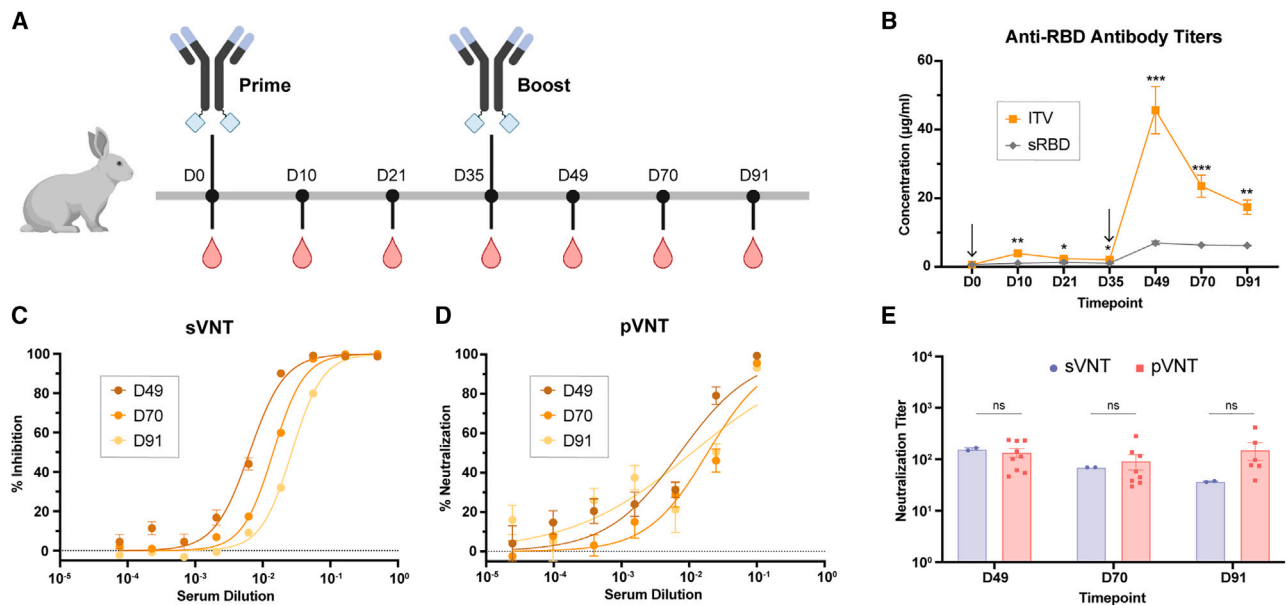


Figure 3. Adjuvant-free ITV immunization in rabbits induces robust and neutralizing anti-RBD responses

(A) Schedule of rabbit immunizations and sampling ($n = 5$ rabbits/group). Schematic created with BioRender.com.

(B) Quantification of anti-RBD IgG titers elicited by unadjuvanted ITV or sRBD immunization in rabbits. Data are represented as the mean \pm SEM and analyzed by Mann-Whitney test (* $p < 0.05$; ** $p < 0.01$; *** $p < 0.001$).

(C and D) Serum neutralization potency against wild-type SARS-CoV-2 (WIV04/2019) at selected time points measured by sVNT (C) and pVNT (D). Data are represented as the mean \pm SEM of at least two experimental replicates assaying sera pooled from rabbits within each group.

(E) Comparison of serum neutralization titers determined by sVNT and pVNT at selected time points, where neutralization titer corresponds to the serum dilution at which 50% inhibition or neutralization is measured. Data are represented as the mean \pm SEM of individual experimental replicates assaying sera pooled from rabbits within each group and analyzed by a Mann-Whitney test.

Inclusion of T cell epitopes in ITV design enhances RBD-specific antibody responses

The incorporation of universally immunogenic T cell epitopes (TCEs) in the ITV creates the potential to enhance immune responses elicited by this vaccine candidate by bypassing population-level MHC class II allelic variation to provide an efficient source of T cell help. To explore the role of TCEs in augmenting ITV immunogenicity, TpD (tetanus and diphtheria toxoid epitopes separated by a cathepsin cleavage site)²⁴ or PADRE (pan HLA-DR-binding epitope)^{22,23} peptide sequences were fused to the light-chain C terminus of the ITV by a short GGS linker, and the induced antibody response elicited in rabbits immunized s.c. with unadjuvanted ITV, ITV-TpD, or ITV-PADRE was compared. Incorporation of either T helper peptide in ITVs nearly doubled the RBD-specific antibody response relative to the ITV without any TCEs (Figure 4A) and further enhanced vaccine-induced serum neutralization as measured by both sVNT and pVNT (Figure 4B). The addition of TCEs enhanced peak (day 49) sera neutralization potency more than 5-fold ($ED_{50} =$

0.0013) as measured by pVNT, with peak antibody responses roughly equivalent to 100 $\mu\text{g/mL}$ of the highly neutralizing therapeutic mAb REGN10987 ($IC_{50} = 0.04$ nM).³¹ To comparatively assess the impact of vaccine administration on ITV immunogenicity, rabbits were also immunized intramuscularly (i.m.) with ITV-TpD. Consistent with previous findings,^{40,41} greater anti-RBD antibody responses were elicited in i.m.-immunized rabbits compared with those immunized s.c. (Figure S3A), and these responses were also accompanied by greater neutralization potency measured by both pVNT and sVNT (Figures S3B and S3C). Collectively, these data support the incorporation of engineered TCEs and i.m. delivery as a strategy to enhance antigen-specific antibody responses in the context of immunotargeting.

Pre-existing immunity to TD enhances neutralizing antibody titers elicited by ITV-TpD

Given it contains TCEs derived from tetanus and diphtheria (TD) toxoids, the TpD peptide provides an opportunity to enhance the

(B) 3.1 Å crystal structure of the c44H10 Fab in complex with HA peptide-bound HLA-DR (HLA-DRA*01:01 [dark blue], HLA-DRB1*04:01 [light blue]). HC, heavy chain; KC, kappa chain.

(C) Buried surface area (BSA) contribution of HLA-DR residues contacted by c44H10 as determined by PDBePISA interface analysis.³³ Residues involved in hydrogen bonds (H) and disulfide bridges (S) are indicated by black dotted lines. Below is the HLA-DR α and β chain sequence diversity of contacted residues from the IPD-IMGT/HLA database in Weblogo representation,^{34,35} where residues from the crystallized allele are black and alternative residues from other alleles are gray. The three residues in the HLA-DR epitope targeted by c44H10 that display slight sequence diversity (α -W168, β -F58, and β -H60) are indicated by boxes and colored in orange. See also Figure S2.

(D) BLI binding of c44H10 to HLA-DR mutants with substitutions in key peripherally contacted residues. Black lines represent measured binding and orange curves correspond to the data fitted to a 1:1 binding model ($R^2 < 0.98$).

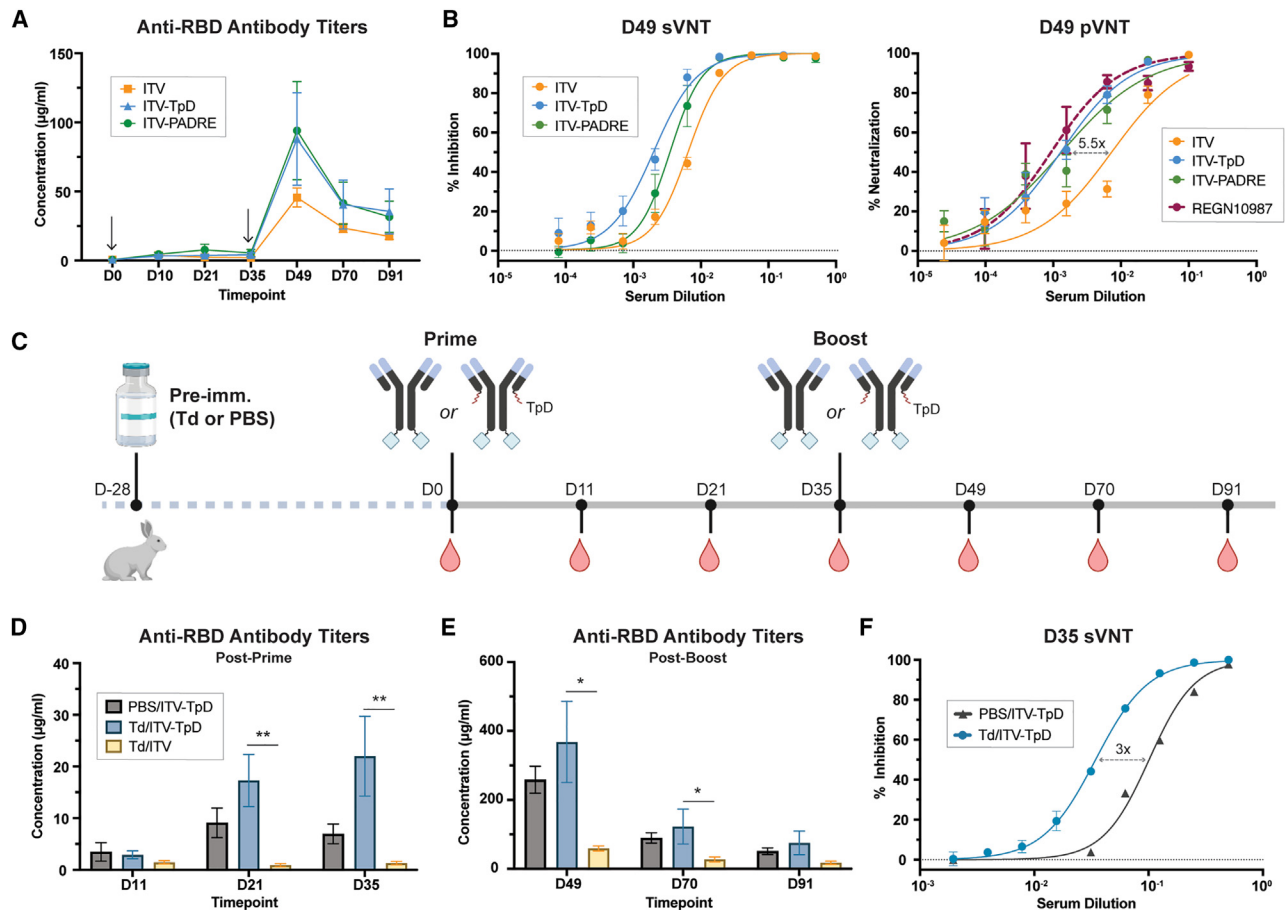


Figure 4. ITV-induced anti-RBD responses are enhanced by engineered T cell epitopes and pre-existing immunity

(A) Anti-RBD IgG titers elicited by unadjuvanted ITV, ITV-TpD, or ITV-PADRE in immunized rabbits measured by ELISA ($n = 5\text{--}10$ rabbits/group). Data are represented as the mean \pm SEM of individual rabbit measurements within each group.

(B) Neutralization potency of vaccine-induced antibody responses measured by sVNT and pVNT, benchmarked to a pre-immunized serum sample to which 100 $\mu\text{g}/\text{mL}$ of mAb REGN10987 was added. Data are represented as the mean \pm SEM of at least two (sVNT) or three (pVNT) experimental replicates.

(C) Immunization schedule to evaluate the role of pre-existing anti-tetanus and diphtheria (TD) toxoid immunity in enhancing ITV-TpD immunogenicity. Schematic created with [BioRender.com](https://www.biorender.com).

(D–F) Quantification (D and E) and neutralization potency (F) of anti-RBD IgG titers elicited in rabbits after one (D and F) or two (E) doses of ITV/ITV-TpD. sVNT data are represented as the mean \pm SEM of experimental duplicates assaying sera pooled from rabbits within each group and were analyzed by Kruskal Wallis followed by Dunn's multiple comparisons test ($*p < 0.05$; $** < 0.01$).

See also [Figure S3](#).

response to foreign antigens delivered on an ITV via its potential to recall helper T cell responses in populations previously immunized against TD.²⁴ To assess whether pre-existing anti-TD immunity could enhance the immunogenicity of TpD-containing ITVs, rabbits were first pre-immunized with either the licensed Sanofi Td Adsorbed vaccine (Td) or PBS and subsequently immunized i.m. with either ITV or ITV-TpD (Figure 4C). Among Td pre-immunized rabbits, significantly higher anti-RBD IgG titers were observed in rabbits immunized with ITV-TpD compared with those immunized with ITV alone (Figures 4D and 4E). Interestingly, antibody responses from both groups immunized with ITV-TpD also displayed higher avidity than those immunized with ITV, suggesting improved quality of the antibody response and presumably reflecting the favorable contribution of TpD to germinal center dynamics and affinity maturation (Fig-

ure S3D). Furthermore, among rabbits immunized with ITV-TpD, the highest induction of antigen-specific antibodies occurred in those previously immunized with Td vaccine, suggesting that immunity established by Td pre-immunization contributed to the enhancement of ITV-TpD immunogenicity. Additionally, Td-pre-immunized rabbits showed enhanced neutralization potency relative to control rabbits, which was particularly apparent after a single dose of ITV-TpD, where higher serum antibody titers were accompanied by a 3-fold increase in neutralization potency as measured by sVNT (Figure 4F).

As an emerging lead, we evaluated the stability of purified ITV-TpD stored at three different temperatures (-20°C , 4°C , and 40°C) for up to 3 weeks. ITV-TpD remained monodisperse and retained RBD structural integrity and binding to MHC class II

even under high thermal stress for prolonged periods of time (Figure S4), demonstrating the high thermostability of this molecule as built on the Ig scaffold. Together, these data emphasize the contribution of TCEs to vaccine immunogenicity and the robustness of the IgG scaffold in protein engineering and vaccine development.

Adjuvant-free ITV-TpD immunization protects ferrets from SARS-CoV-2 challenge

To assess the ability of ITV-TpD immunization to protect from SARS-CoV-2 challenge, ferrets were immunized i.m. with 50 μ g unadjuvanted ITV-TpD or an equimolar dose of Alum-adjuvanted sRBD (sRBD-Alum) in a prime-boost regimen and were subsequently challenged intranasally with 10^6 PFU live SARS-CoV-2 virus (Wuhan-Hu-1) at 2 weeks post-boost (Figure 5A). Anti-RBD antibody titers elicited by immunization were significantly greater in ferrets immunized with unadjuvanted ITV-TpD than sRBD-Alum, especially after one dose of vaccine (Figure 5B). Correspondingly, sera from the unadjuvanted ITV-TpD group displayed greater virus neutralization potency than that of the sRBD-Alum group, as measured by plaque reduction neutralization assay (Figure 5C).

Measurements of viral titers from nasal washes by qRT-PCR in the 10 days following challenge revealed a marked reduction in SARS-CoV-2 viral titers in both the unadjuvanted ITV-TpD- and sRBD-Alum-immunized groups compared with the control PBS group (Figure 5D). These data were additionally confirmed by the quantification of virus isolated from nasal washes of challenged animals, with lower viral titers measured in ferrets immunized with unadjuvanted ITV-TpD and sRBD-Alum compared with the control group (Figure 5E). Post-challenge monitoring of symptoms confirmed the establishment of SARS-CoV-2 infection in control ferrets, which developed signs of disease around day 7–10 post-challenge (Figure 5F). While clinical signs of disease were observed in some animals of the sRBD-Alum group, all ferrets in the unadjuvanted ITV-TpD group remained healthy and responsive throughout the duration of the study. Together, these data support the ability of unadjuvanted ITV-TpD to protect ferrets from SARS-CoV-2-associated disease and elicit robust neutralizing anti-RBD responses at levels surpassing Alum-adjuvanted RBD.

Modular ITV design allows inclusion of multiple RBDs to achieve broad sarbecovirus neutralization

To address the need of next-generation COVID-19 vaccines to broadly counter continuously emerging VOCs, we assessed the ability of ITVs to simultaneously carry RBD antigens from two distinct sarbecoviruses. Specifically, the SARS-CoV-2 and SARS-CoV-1 spike protein RBDs were, respectively, fused to the c44H10 IgG heavy and light chains (Figure 6A). With consideration to our results on the importance of TCEs for ITV immunogenicity, TpD was also fused to the C terminus of the SARS-CoV-1 RBD on the ITV light chain. Biantigenic ITV-TpD migration in SDS-PAGE under reducing conditions revealed heavy- and light-chain bands at 75 and 50 kDa, respectively, consistent with the fusion of an RBD to each antibody chain (Figure 6B). A panel of non-cross-reactive mAbs was used in flow cytometry experiments to assess the proper folding of both RBD antigens

on the ITV-TpD. SARS-CoV-1 RBD-specific mAbs m396 and 80R^{42,43} only displayed binding to biantigenic ITV-TpD, whereas SARS-CoV-2 RBD-specific mAbs REGN10987 and REGN10933³¹ bound to both mono- and biantigenic ITV-TpD molecules (Figure 6C), confirming the ability of the ITV platform to successfully co-display diverse and conformationally intact RBD antigens.

Rabbits immunized with biantigenic ITV-TpD elicited significantly higher anti-SARS-CoV-1 RBD responses than those immunized with mono-antigenic ITV-TpD (Figure 6D). Importantly, the enhancement in anti-SARS-CoV-1 responses elicited by biantigenic ITV-TpD did not compromise the development of anti-SARS-CoV-2 antibody responses, which were equivalent in both mono- and biantigenic groups. Interestingly, mono-antigenic ITV-TpD elicited a measurable anti-SARS-CoV-1 RBD response despite not having SARS-CoV-1 RBD on the immunogen, suggesting the elicitation of antibodies cross-reactive between both SARS-CoV-1 and SARS-CoV-2 RBDs. Roughly equivalent levels of anti-SARS-CoV-1 and SARS-CoV-2 antibodies were elicited by biantigenic ITV-TpD immunization, suggesting that both sites of RBD incorporation on the c44H10 IgG scaffold (heavy chain and/or light chain) were equally effective for antigen immunogenicity. Both immunogens elicited robust neutralizing antibody responses against wild-type SARS-CoV-2 and retained neutralization against a wide range of VOCs, including the highly divergent Omicron BA.1 and BA.5 variants (Figures 6E and S5B). In contrast, significantly higher neutralization against SARS-CoV-1 was conferred by the incorporation of the SARS-CoV-1 RBD on the biantigenic ITV-TpD (Figures 6E and S5A). Collectively, these data support the modular nature of the ITV scaffold as an effective adjuvant-free vaccine platform for the delivery and induction of robust antibody responses against diverse RBD antigens.

DISCUSSION

Immunotargeting as an approach to vaccine design has previously been explored in the context of different antigens and target molecules on the surface of various APC subsets.^{13,44,45} Targeting to MHC class II has been the most widely evaluated, with several studies having reported the elicitation of antigen-specific humoral responses enhanced relative to administration of antigen alone.^{12,14,46} In addition, antigen unlinked to but co-administered with MHC class II-targeting mAb fails to induce significant IgG antibody responses to the antigen.^{11,15–17,47,48} In mice, antigen linked to an isotype-matched antibody of irrelevant specificity does not elicit antigen-specific antibody responses, and matching the specificity of the targeting antibody to the recipient's MHC haplotype was demonstrated to be essential for responsiveness,^{11,49} attributing the observed effect to the targeting property of the scaffold antibody used.

The ITV described herein builds upon these principles, eliciting robust neutralizing antibody responses against the SARS-CoV-2 RBD even in the absence of adjuvant. Interestingly, a recent report described a vaccine candidate targeting the SARS-CoV-2 spike protein RBD to MHC class II by use of an alpaca-derived nanobody (VHH_{MHCII}).¹² However, the elicited robust humoral and cellular immunity against SARS-CoV-2 and its variants

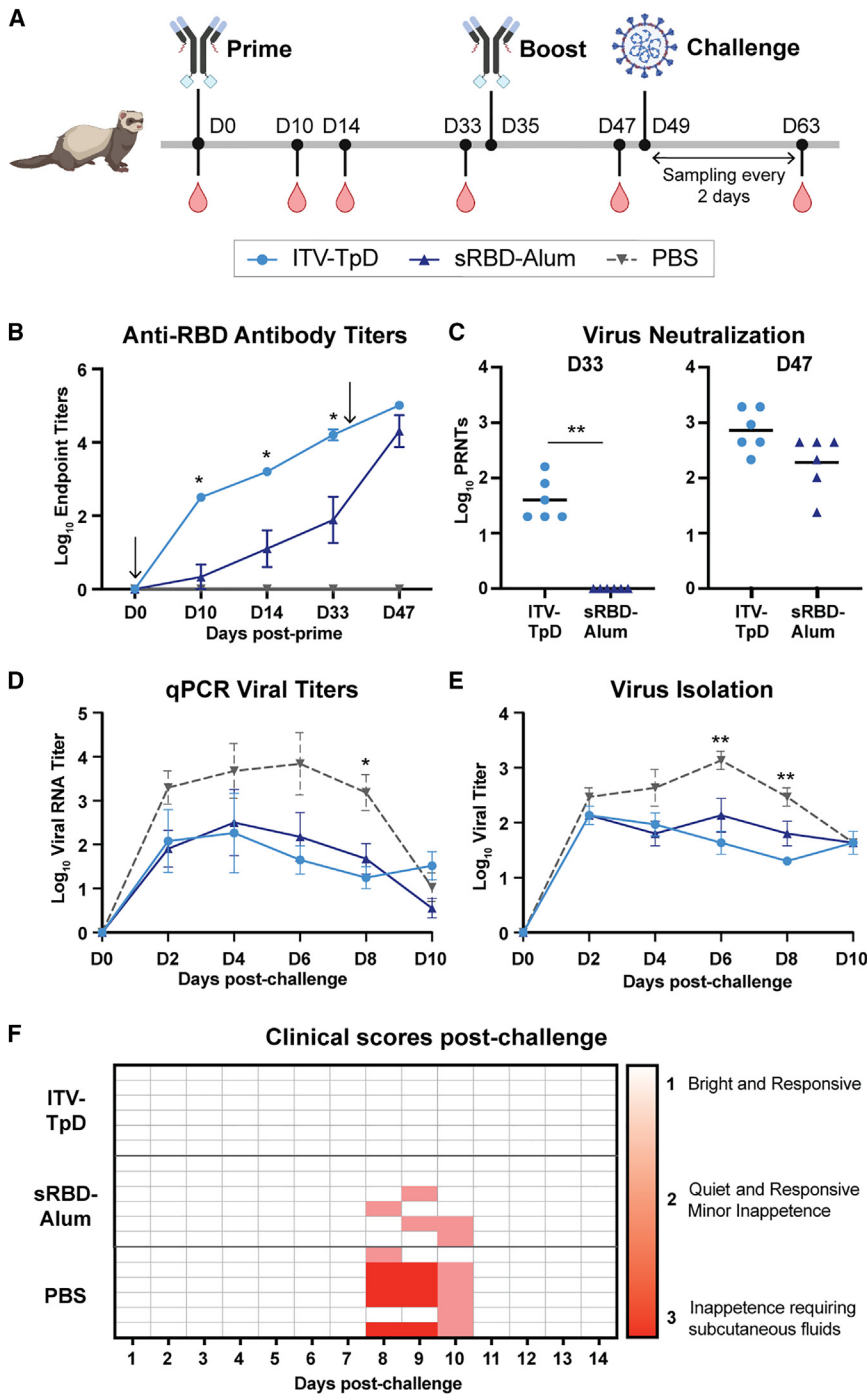


Figure 5. Antibody responses elicited by ITV-TpD immunization in ferrets protect against SARS-CoV-2 challenge

(A) Schedule of ferret immunization, sampling, and challenge (n = 6 ferrets/group). Schematic created with BioRender.com.

(B) Anti-RBD endpoint titers elicited by ITV-TpD or sRBD-Alum immunization prior to challenge as measured by ELISA. Asterisks indicate significant differences between ITV-TpD and sRBD-Alum groups. Data analyzed by Kruskal-Wallis followed by Dunn's multiple comparisons test (*p < 0.05; **p < 0.01).

(C) Serum neutralization titers of live SARS-CoV-2 virus measured by plaque reduction neutralization assay after one (D33) or two (D47) vaccine doses. Data analyzed by Mann-Whitney test (**p < 0.01). (D and E) qRT-PCR detection of viral RNA (D) and virus isolation to quantify viable virus (E) from post-challenge nasal washes collected from ferrets. Asterisks indicate significant differences between ITV-TpD and PBS groups. Data analyzed by Kruskal-Wallis followed by Dunn's multiple comparisons test (*p < 0.05; **p < 0.01).

(F) Development of symptoms in ferrets in the 14 days post-challenge as assessed by a blind observer.

For all panels, data are represented as the mean ± SEM of individual ferret measurements within each group.

ously immunized with mRNA-LNP vaccine was recently shown to be highly effective in generating mucosal humoral immune responses.⁵⁰ Thus, the advantages of developing ITVs are apparent for the immunization of both antigen-experienced and antigen-naïve populations, emphasizing the potential to be used in both priming and boosting scenarios. A systemic head-to-head comparison of various ITV modalities targeting different APC receptors remains to be explored to determine whether one receptor surpasses the others for the elicitation of neutralizing antibody responses or whether the simultaneous targeting of multiple receptors could synergistically enhance this response.

Though it is one of the best-characterized APC receptors for immunotargeting, the extreme polymorphism of the MHC

required co-administration of poly(dI-dC) with anti-CD40. The potential of antigen immunotargeting for a COVID-19 vaccine has also been explored in the context of other APC receptors. In one instance, a vaccine targeting the SARS-CoV-2 spike protein RBD to CD40 molecules expressed on APCs conferred protection against further COVID-19 infection in convalescent macaques when administered without adjuvant.¹³ Furthermore, intranasal unadjuvanted spike protein boosting in mice previ-

locus represents a substantial challenge for the development of an ITV that is broadly reactive in the human population. Here, our molecular characterization of mAb 44H10 builds on prior literature establishing it as a pan-HLA-DR mAb²⁰ and provides important insights into the ability of 44H10 to overcome HLA-DR diversity through targeting a highly conserved epitope, further supporting the use of this antibody for immunotargeting across diverse human populations. In fact, these molecular

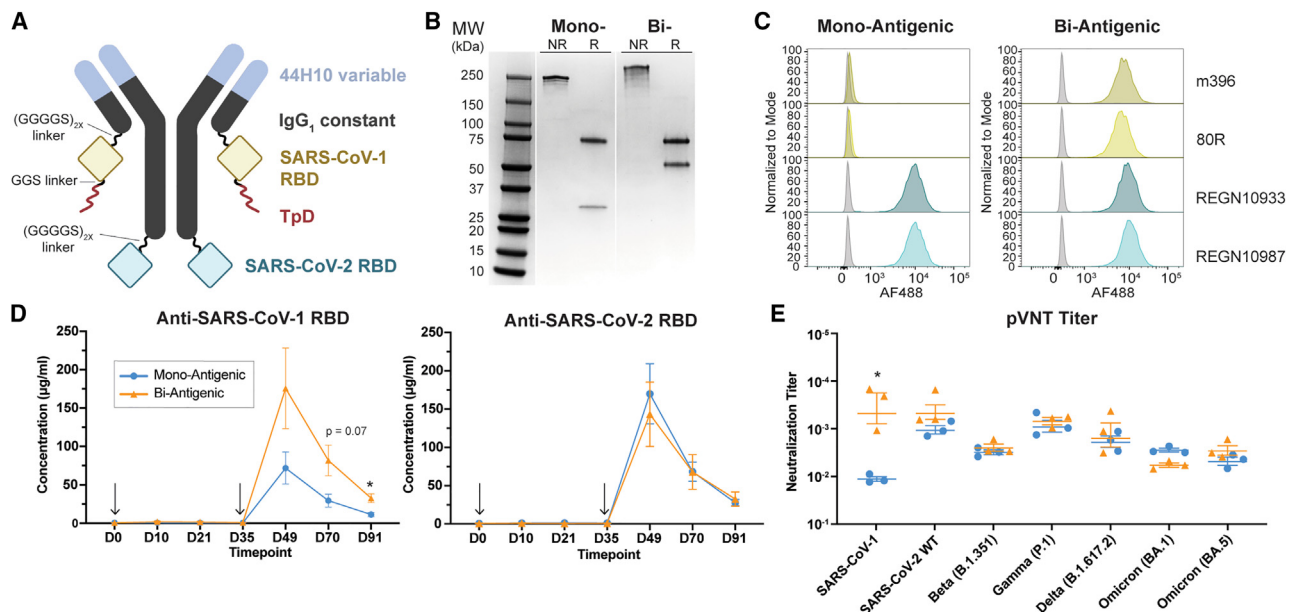


Figure 6. Modular ITV design allows for inclusion of diverse antigens for broad virus neutralization

(A) Schematic representation of the biantigenic ITV incorporating RBDs from both SARS-CoV-1 and SARS-CoV-2 and the T helper peptide TpD. Created with BioRender.com.

(B) SDS-PAGE of purified mono- and biantigenic ITVs under NR and R conditions.

(C) Detection of mAbs targeting the SARS-CoV-1 RBD (m396, 80R) or SARS-CoV-2 RBD (REGN10933, REGN10987) binding to mono- and biantigenic ITV by flow cytometry.

(D) Anti-SARS-CoV-1 RBD and anti-SARS-CoV-2 anti-RBD IgG titers elicited by unadjuvanted mono- or biantigenic ITV-TpD in immunized rabbits measured by ELISA ($n = 5$ rabbits/group). Data are represented as the mean \pm SEM of individual rabbit measurements within each group and analyzed by Mann-Whitney test ($*p < 0.05$).

(E) Day 49 (peak) pVNT titers against SARS-CoV-1 and SARS-CoV-2 strains measured in rabbits immunized with either mono- or biantigenic ITV-TpD, where neutralization titer corresponds to the serum dilution at which 50% pseudovirus neutralization is measured. Data are represented as the mean \pm SEM of experimental triplicates assaying sera pooled from rabbits within each group and were analyzed by Mann-Whitney test ($*p < 0.05$).

See also Figure S5.

insights were confirmed by the broad reactivity of the antibody against a random set of 100 different PBMC samples, likely capturing considerable HLA-DR diversity.

In the absence of adjuvant, each component of the immunogen plays an important role in maximizing its immunogenicity, including antigen multimerization. It had previously been reported that recombinant fusion of the SARS-CoV-2 RBD to an Fc scaffold, effectively dimerizing RBDs and retaining antibody Fc-mediated interactions, significantly improved the humoral response to this antigen compared with monomeric RBDs.⁵¹ Beyond dimerization, several groups have investigated a variety of nanoparticle platforms for higher-order antigen multimerization by integrating between 1 and 60 copies of RBD per vaccine particle, highlighting the potential of such platforms for the elicitation of superior and broader antigen-specific antibody responses.^{52–58} Thus, the use of an IgG platform enabling the incorporation of more than one antigen per vaccine molecule can effectively enhance immunogenicity through a combination of both multivalent antigen display as well as targeted antigen delivery. As expected for the immunoglobulin scaffold, we found a high thermostability for the ITV, which retained MHC class II-targeting ability and structural integrity of its fused RBD component for weeks under thermal stress. Potentially, such

characteristics would lower the requirements for extensive cold-chain infrastructure for vaccine storage and distribution. Similarly, the mAb-like nature of the ITV should also lend itself to the economical large-scale production of such vaccines using the methodologies developed for mAb manufacturing. These features could facilitate vaccine production and deployment in regions where storage and cost have impeded vaccine access. Indeed, effective management of COVID-19 in the years to come will likely hinge on widespread access to safe, effective, and low-cost vaccines.

Beyond immunotargeting and antigen multimerization, there is accumulating evidence for the importance of TCEs in shaping immune responses following vaccination through the provision of T cell help, which, in turn, supports the induction of downstream antibody responses. Our data substantiate previous reports, demonstrating that the incorporation of either synthetic (PADRE) or naturally derived (TpD) TCEs considerably enhance RBD-specific antibody responses elicited by ITV vaccination. Vaccination against tetanus and diphtheria (TD) is known to induce long-lived T and B cell memory, and global vaccination programs against both diseases leading to widespread vaccine coverage have resulted in drastic declines in disease incidence and mortality.^{59–61} Prior studies have shown that the inclusion

of TpD successfully elicits recall responses to prior TD immunization in non-human primate models.²⁴ In addition to the benefits of including TpD in ITV design for the immunization of a TD-naive subject, our data indicate that TpD may additionally leverage pre-existing helper T cell responses in a TD-experienced host. Thus, our work supports the use of TpD both as a T helper peptide and as an effective tool to harness pre-existing immunity to tetanus and/or diphtheria toxoids to enhance vaccine immunogenicity for ITVs. How dosage and timing of Td pre-immunization might alter TpD-mediated enhancement of antibody responses remains an area of future exploration.

While the global response to the COVID-19 pandemic resulted in the deployment of vaccines and therapeutics targeting SARS-CoV-2 in record-breaking time, the emergence of VOCs has significantly impacted the efficacy of such interventions developed in the early phases of the pandemic.^{62–64} Thus, the development of vaccine platforms that can provide breadth of coverage against multiple viral strains would represent a significant advancement for counteracting rapidly evolving pathogens. Here, neutralization against a wide range of SARS-CoV-2 VOCs was conferred by the RBD-based mono-antigenic ITV-TpD immunogen following an unadjuvanted two-dose immunization regimen in rabbits. Notably, antibodies elicited in sera following the second dose of ITV-TpD cross-neutralized the highly divergent and antigenically distinct Omicron BA.1 and BA.5 variants^{65,66} with 2- and 4-fold reductions in neutralization titers relative to wild-type SARS-CoV-2, respectively. In contrast, many licensed vaccines—including the COVID-19 mRNA vaccines BNT162b2 and mRNA-1273, which utilize the prefusion stabilized full spike glycoprotein—have been reported to exhibit significantly reduced serum neutralization against SARS-CoV-2 Omicron following prime-boost immunization, with >20-fold reduction in neutralizing antibody titers relative to wild-type D614G SARS-CoV-2 at 2 or 3 weeks post-boost.^{67–69} We additionally provide proof of concept for the ability of the ITV platform to incorporate RBD antigens from at least two different sarbecovirus strains (SARS-CoV-2 and SARS-CoV-1) and elicit antibody responses with broad sarbecovirus-neutralizing activity. Though this work only describes the engineering of a biantigenic ITV, the modular nature of the ITV platform combined with bispecific antibody technology could enable the fusion of up to four different antigenic sequences on a single molecule, providing a compelling scaffold for multivalent subunit-based vaccines against future pandemic challenges in the context of viral diversity (e.g., coronaviruses, influenza, etc.).

Emerging SARS-CoV-2 variants continue to highlight the need for global COVID-19 vaccination coverage and strategies that induce immune responses with increased potency and breadth. As a platform, the ITV lays the foundations for a modular and multivalent subunit-based vaccination strategy with the ability to circumvent the need for extrinsic adjuvant systems. Through immunotargeting and specific immunogen engineering, the ITV platform can potentially alleviate development challenges associated with classical subunit vaccines to facilitate vaccine manufacturing, deployment, and accessibility during pandemic responses. Furthermore, the simplicity of the ITV design might lend itself to antigen delivery possibilities across multiple vaccine modalities, including protein subunit, mRNA, or viral vectors.

Limitations of the study

While the present work introduces the ITV as a promising adjuvant-free strategy for the design of next-generation subunit vaccines, several mechanistic questions remain to be answered. In this regard, research pertaining to mechanisms of action may benefit from being carried out in the context of mouse and/or primate models, where more extensive validated immunological reagents are available for in-depth characterization of immune responses. For this purpose, development of a 44H10-like antibody that cross-reacts with mouse MHC class II would be particularly beneficial. Further development of the ITV platform may also benefit from the humanization of the 44H10 antibody sequence to minimize the risk of immunogenicity of the antibody scaffold downstream, with the ultimate goal of focusing the response on the immunotargeted antigen.

STAR★METHODS

Detailed methods are provided in the online version of this paper and include the following:

- **KEY RESOURCES TABLE**
- **RESOURCE AVAILABILITY**
 - Lead contact
 - Materials availability
 - Data and code availability
- **EXPERIMENTAL MODEL AND SUBJECT DETAILS**
 - Mammalian cell lines and culture conditions
 - Rabbits
 - Ferrets
 - Human PBMCs
- **METHOD DETAILS**
 - Plasmid design and synthesis
 - Expression and purification of recombinant ITVs and anti-RBD mAbs
 - Expression and purification of recombinant c44H10 Fab
 - Expression and purification of recombinant SARS-CoV-2 RBD and hACE2
 - Design, expression and purification of recombinant MHC Class II
 - Dynamic Light Scattering of RBD, c44H10 IgG and ITV
 - Negative-stain electron microscopy
 - Fluorescent labeling of anti-RBD mAbs for flow cytometry
 - Flow cytometry for confirmation of MHC class II-targeting and RBD structural integrity
 - Flow cytometry for 44H10 binding to human PBMCs
 - Biolayer interferometry for measurement of recombinant MHC class II-c44H10/ITV binding
 - Biolayer interferometry for measurement of ITV binding to hACE2
 - Co-crystallization and structure determination of the c44H10 Fab-MHC class II complex
 - Endotoxin measurements and removal for *in vivo* studies
 - Rabbit immunizations

- ELISA measurement of anti-RBD titers elicited in rabbits
- ELISA measurement of antibody avidity index
- Surrogate virus neutralization assay (sVNT)
- Pseudovirus production
- Pseudovirus neutralization assay (pVNT)
- Ferret immunizations and challenge
- ELISA measurement of anti-RBD titers elicited in ferrets
- Plaque reduction neutralization titer (PRNT) assay
- RNA extraction from nasal washes
- RT-qPCR for measurement of viral titers in nasal washes
- Virus isolation from nasal washes
- **QUANTIFICATION AND STATISTICAL ANALYSIS**

SUPPLEMENTAL INFORMATION

Supplemental information can be found online at <https://doi.org/10.1016/j.celrep.2023.112391>.

ACKNOWLEDGMENTS

We thank Tahir Maqbool at Cedarlane Laboratories for the handling and immunization of rabbits, as well as Eddie Johnson, Joel Kooistra, and Ali Lessan for the coordination and execution of *in vivo* studies. We thank Dr. Valerie Smid and the Animal Care Staff at CFIA-NCFAD for the animal care of the ferrets. We are also grateful to Dr. Bradley Pickering for providing us with the SARS-CoV-2 virus used for ferret challenge experiments. We furthermore thank Elaine Thai for support provided in the processing and validation of crystallographic data and Clare Burn Aschner for helpful suggestions for the analysis of sVNT data. This work was supported by a Master's Canada Graduate Scholarship (OGS), and E.S. is supported by a Master's Canada Graduate Scholarship (CGS-M). I.K. is supported by a Hospital for Sick Children Restracom Postdoctoral Fellowship, and E.R. is supported by the European Union's Horizon 2020 research and innovation program under Marie Skłodowska-Curie grant 790012. The BLI and DLS instruments were accessed at the Structural & Biophysical Core Facility, the analytical cytometers at the Flow Cytometry Facility, and the electron microscope at the Nanoscale Biomedical Imaging Facility at The Hospital for Sick Children, supported by the Canada Foundation for Innovation and Ontario Research Fund. X-ray diffraction experiments were performed at GM/CA@APS, which has been funded in whole or in part with federal funds from the National Cancer Institute (ACB-12002) and the National Institute of General Medical Sciences (AGM-12006). The Eiger 16M detector at GM/CA-XSD was funded by NIH grant S10 OD012289. This research used resources of the Advanced Photon Source, a US Department of Energy (DOE) Office of Science user facility operated for the DOE Office of Science by Argonne National Laboratory under contract DE-AC02-06CH11357. The graphical abstract and select figures were created with [BioRender.com](https://www.biorender.com).

AUTHOR CONTRIBUTIONS

Experimental design was collaborative between all co-authors. Experiments were conducted by A.K., E.S., J.S., K.M., K.F.B., I.K., and E.R. The manuscript was written by A.K., E.S., and J.-P.J., and edited by all co-authors. Funding was secured by D.R.B., B.B., and J.-P.J.

DECLARATION OF INTERESTS

A patent application has been filed that relates to this work.

Received: November 9, 2022

Revised: February 14, 2023

Accepted: March 29, 2023

Published: April 3, 2023

REFERENCES

1. Polack, F.P., Thomas, S.J., Kitchin, N., Absalon, J., Gurtman, A., Lockhart, S., Perez, J.L., Pérez Marc, G., Moreira, E.D., Zerbini, C., et al. (2020). Safety and efficacy of the BNT162b2 mRNA covid-19 vaccine. *N. Engl. J. Med.* *383*, 2603–2615. <https://doi.org/10.1056/NEJM0A2034577>.
2. Baden, L.R., El Sahly, H.M., Essink, B., Kotloff, K., Frey, S., Novak, R., Diekmert, D., Spector, S.A., Rouphael, N., Creech, C.B., et al. (2021). Efficacy and safety of the mRNA-1273 SARS-CoV-2 vaccine. *N. Engl. J. Med.* *384*, 403–416. <https://doi.org/10.1056/NEJM0A2035389>.
3. Dzau, V.J., Balatbat, C.A., and Offodile, A.C. (2022). Closing the global vaccine equity gap: equitably distributed manufacturing. *Lancet* *399*, 1924–1926. [https://doi.org/10.1016/S0140-6736\(22\)00793-0](https://doi.org/10.1016/S0140-6736(22)00793-0).
4. Hunter, D.J., Abdool Karim, S.S., Baden, L.R., Farrar, J.J., Hamel, M.B., Longo, D.L., Morrissey, S., and Rubin, E.J. (2022). Addressing vaccine inequity — covid-19 vaccines as a global public good. *N. Engl. J. Med.* *386*, 1176–1179. <https://doi.org/10.1056/NEJME2202547>.
5. Pulendran, B., and Ahmed, R. (2011). Immunological mechanisms of vaccination. *Nat. Immunol.* *12*, 509–517. <https://doi.org/10.1038/ni.2039>.
6. Petrovsky, N. (2015). Comparative safety of vaccine adjuvants: a summary of current evidence and future needs. *Drug Saf.* *38*, 1059–1074. <https://doi.org/10.1007/s40264-015-0350-4>.
7. Sun, Y., Gruber, M., and Matsumoto, M. (2012). Overview of global regulatory toxicology requirements for vaccines and adjuvants. *J. Pharmacol. Toxicol. Methods* *65*, 49–57. <https://doi.org/10.1016/j.vascn.2012.01.002>.
8. Pulendran, B., S Arunachalam, P., O'Hagan, D.T., and O'Hagan, D.T. (2021). Emerging concepts in the science of vaccine adjuvants. *Nat. Rev. Drug Discov.* *20*, 454–475. <https://doi.org/10.1038/s41573-021-00163-y>.
9. Martín, R.S., and Briones, R. (1999). Industrial uses and sustainable supply of Quillaja saponaria (Rosaceae) saponins. *Econ. Bot.* *53*, 302–311. <https://doi.org/10.1007/BF02866642>.
10. Wang, P. (2021). Natural and synthetic saponins as vaccine adjuvants. *Vaccines* *9*, 222. <https://doi.org/10.3390/VACCINES9030222>.
11. Carayanniotis, G., and Barber, B.H. (1987). Adjuvant-free IgG responses induced with antigen coupled to antibodies against class II MHC. *Nature* *327*, 59–61. <https://doi.org/10.1038/327059a0>.
12. Pishesha, N., Harmand, T.J., Rothlauf, P.W., Praest, P., Alexander, R.K., van den Doel, R., Liebeskind, M.J., Vakaki, M.A., McCaul, N., Wijne, C., et al. (2021). A class II MHC-targeted vaccine elicits immunity against SARS-CoV-2 and its variants. *Proc. Natl. Acad. Sci. USA* *118*, e2116147118. <https://doi.org/10.1073/PNAS.2116147118>.
13. Marlin, R., Godot, V., Cardinaud, S., Galhaut, M., Coleon, S., Zurawski, S., Dereuddre-Bosquet, N., Cavarelli, M., Gallouët, A.S., Maisonnasse, P., et al. (2021). Targeting SARS-CoV-2 receptor-binding domain to cells expressing CD40 improves protection to infection in convalescent macaques. *Nat. Commun.* *12*, 5215. <https://doi.org/10.1038/s41467-021-25382-0>.
14. Andersen, T.K., Huszthy, P.C., Gopalakrishnan, R.P., Jacobsen, J.T., Fauskanger, M., Tveita, A.A., Grødeland, G., and Bogen, B. (2019). Enhanced germinal center reaction by targeting vaccine antigen to major histocompatibility complex class II molecules. *npj Vaccines* *4*, 9. <https://doi.org/10.1038/s41541-019-0101-0>.
15. Skea, D.L., and Barber, B.H. (1992). Adjuvant-independent induction of immune responses by antibody-mediated targeting of protein and peptide antigens. In *Research in Immunology* (Elsevier Masson), pp. 568–582. [https://doi.org/10.1016/0923-2494\(92\)80071-R](https://doi.org/10.1016/0923-2494(92)80071-R).
16. Skea, D.L., Douglas, A.R., Skehel, J.J., and Barber, B.H. (1993). The immunotargeting approach to adjuvant-independent immunization with

- influenza haemagglutinin. *Vaccine* 11, 994–1002. [https://doi.org/10.1016/0264-410X\(93\)90123-F](https://doi.org/10.1016/0264-410X(93)90123-F).
17. Skea, D.L., and Barber, B.H. (1993). Studies of the adjuvant-independent antibody response to immunotargeting. Target structure dependence, isotype distribution, and induction of long term memory. *J. Immunol.* 151, 3557–3568.
 18. Barber, B.H. (1997). The immunotargeting approach to adjuvant-independent subunit vaccine design. *Semin. Immunol.* 9, 293–301. <https://doi.org/10.1006/smim.1997.0085>.
 19. Ho, J., Uger, R.A., Zwick, M.B., Luscher, M.A., Barber, B.H., and MacDonald, K.S. (2005). Conformational constraints imposed on a pan-neutralizing HIV-1 antibody epitope result in increased antigenicity but not neutralizing response. *Vaccine* 23, 1559–1573. <https://doi.org/10.1016/j.vaccine.2004.09.037>.
 20. Dubiski, S., Cinader, B., Chou, C.T., Charpentier, L., and Letarte, M. (1988). Cross-reaction of a monoclonal antibody to human MHC class II molecules with rabbit B cells. *Mol. Immunol.* 25, 713–718. [https://doi.org/10.1016/0161-5890\(88\)90107-1](https://doi.org/10.1016/0161-5890(88)90107-1).
 21. Quackenbush, E.J., and Letarte, M. (1985). Identification of several cell surface proteins of non-T, non-B acute lymphoblastic leukemia by using monoclonal antibodies. *J. Immunol.* 134, 1276–1285.
 22. Franke, E.D., Hoffman, S.L., Sacci, J.B., Wang, R., Charoenvit, Y., Appella, E., Chesnut, R., Alexander, J., Del Guercio, M.F., and Sette, A. (1999). Pan DR binding sequence provides T-cell help for induction of protective antibodies against *Plasmodium yoelii* sporozoites. *Vaccine* 17, 1201–1205. [https://doi.org/10.1016/S0264-410X\(98\)00341-7](https://doi.org/10.1016/S0264-410X(98)00341-7).
 23. Alexander, J., del Guercio, M.-F., Maewal, A., Qiao, L., Fikes, J., Chesnut, R.W., Paulson, J., Bundle, D.R., DeFrees, S., and Sette, A. (2000). Linear PADRE T helper epitope and carbohydrate B cell epitope conjugates induce specific high titer IgG antibody responses. *J. Immunol.* 164, 1625–1633. <https://doi.org/10.4049/jimmunol.164.3.1625>.
 24. Fraser, C.C., Altmeyer, D.H., Ilyinskii, P., Pittet, L., LaMothe, R.A., Keegan, M., Johnston, L., and Kishimoto, T.K. (2014). Generation of a universal CD4 memory T cell recall peptide effective in humans, mice and non-human primates. *Vaccine* 32, 2896–2903. <https://doi.org/10.1016/j.vaccine.2014.02.024>.
 25. Park, H.Y., Tan, P.S., Kavishna, R., Ker, A., Lu, J., Chan, C.E.Z., Hanson, B.J., MacAry, P.A., Caminschi, I., Shortman, K., et al. (2017). Enhancing vaccine antibody responses by targeting Clec9A on dendritic cells. *npj Vaccines* 2, 31–11. <https://doi.org/10.1038/s41541-017-0033-5>.
 26. Baum, A., Fulton, B.O., Wloga, E., Copin, R., Pascal, K.E., Russo, V., Giordano, S., Lanza, K., Negron, N., Ni, M., et al. (2020). Antibody cocktail to SARS-CoV-2 spike protein prevents rapid mutational escape seen with individual antibodies. *Science* 369, 1014–1018. <https://doi.org/10.1126/SCIENCE.ABD0831>.
 27. Barnes, C.O., Jette, C.A., Abernathy, M.E., Dam, K.M.A., Esswein, S.R., Gristick, H.B., Malyutin, A.G., Sharaf, N.G., Huey-Tubman, K.E., Lee, Y.E., et al. (2020). SARS-CoV-2 neutralizing antibody structures inform therapeutic strategies. *Nature* 588, 682–687. <https://doi.org/10.1038/S41586-020-2852-1>.
 28. Tian, X., Li, C., Huang, A., Xia, S., Lu, S., Shi, Z., Lu, L., Jiang, S., Yang, Z., Wu, Y., and Ying, T. (2020). Potent binding of 2019 novel coronavirus spike protein by a SARS coronavirus-specific human monoclonal antibody. *Emerg. Microbes Infect.* 9, 382–385. <https://doi.org/10.1080/22221751.2020.1729069>.
 29. Yuan, M., Wu, N.C., Zhu, X., Lee, C.C.D., So, R.T.Y., Lv, H., Mok, C.K.P., and Wilson, I.A. (2020). A highly conserved cryptic epitope in the receptor binding domains of SARS-CoV-2 and SARS-CoV. *Science* 368, 630–633. <https://doi.org/10.1126/science.abb7269>.
 30. Zost, S.J., Gilchuk, P., Case, J.B., Binshtein, E., Chen, R.E., Nkolola, J.P., Schäfer, A., Reidy, J.X., Trivette, A., Nargi, R.S., et al. (2020). Potently neutralizing and protective human antibodies against SARS-CoV-2. *Nature* 584, 443–449. <https://doi.org/10.1038/s41586-020-2548-6>.
 31. Hansen, J., Baum, A., Pascal, K.E., Russo, V., Giordano, S., Wloga, E., Fulton, B.O., Yan, Y., Koon, K., Patel, K., et al. (2020). Studies in humanized mice and convalescent humans yield a SARS-CoV-2 antibody cocktail. *Science* 369, 1010–1014. <https://doi.org/10.1126/SCIENCE.ABD0827>.
 32. Shiina, T., Hosomichi, K., Inoko, H., and Kulski, J.K. (2009). The HLA genomic loci map: expression, interaction, diversity and disease. *J. Hum. Genet.* 54, 15–39. <https://doi.org/10.1038/jhg.2008.5>.
 33. Krissinel, E., and Henrick, K. (2007). Inference of macromolecular Assemblies from crystalline state. *J. Mol. Biol.* 372, 774–797. <https://doi.org/10.1016/J.JMB.2007.05.022>.
 34. Robinson, J., Barker, D.J., Georgiou, X., Cooper, M.A., Flicek, P., and Marsh, S.G.E. (2020). IPD-IMGT/HLA database. *Nucleic Acids Res.* 48, D948–D955. <https://doi.org/10.1093/NAR/GKZ950>.
 35. Crooks, G.E., Hon, G., Chandonia, J.M., and Brenner, S.E. (2004). WebLogo: a sequence Logo generator. *Genome Res.* 14, 1188–1190. <https://doi.org/10.1101/GR.849004>.
 36. Tan, C.W., Chia, W.N., Qin, X., Liu, P., Chen, M.I.C., Tiu, C., Hu, Z., Chen, V.C.W., Young, B.E., Sia, W.R., et al. (2020). A SARS-CoV-2 surrogate virus neutralization test based on antibody-mediated blockage of ACE2–spike protein–protein interaction. *Nat. Biotechnol.* 38, 1073–1078. <https://doi.org/10.1038/s41587-020-0631-z>.
 37. Abe, K.T., Li, Z., Samson, R., Samavarchi-Tehrani, P., Valcourt, E.J., Wood, H., Budyłowski, P., Dupuis, A.P., Girardin, R.C., Rathod, B., et al. (2020). A simple protein-based surrogate neutralization assay for SARS-CoV-2. *JCI Insight* 5, e142362. <https://doi.org/10.1172/JCI.INSIGHT.142362>.
 38. Crawford, K.H., Eguia, R., Dingens, A.S., Loes, A.N., Malone, K.D., Wolf, C.R., Chu, H.Y., Alejandra Tortorici, M., Velesler, D., Murphy, M., et al. (2020). Protocol and reagents for pseudotyping lentiviral particles with SARS-CoV-2 Spike protein for neutralization assays. Preprint at bioRxiv. <https://doi.org/10.1101/2020.04.20.051219>.
 39. Liu, L., Wang, P., Nair, M.S., Yu, J., Rapp, M., Wang, Q., Luo, Y., Chan, J.F.W., Sahi, V., Figueroa, A., et al. (2020). Potent neutralizing antibodies against multiple epitopes on SARS-CoV-2 spike. *Nature* 58, 450–456. <https://doi.org/10.1038/s41586-020-2571-7>.
 40. Techawiwattanaboon, T., Barnier-Quer, C., Palaga, T., Jacquet, A., Collin, N., Sangjun, N., Komane, P., and Patarakul, K. (2020). A comparison of intramuscular and subcutaneous administration of LigA subunit vaccine adjuvanted with neutral liposomal formulation containing monophosphoryl lipid A and QS21. *Vaccines* 8, 494. <https://doi.org/10.3390/VAC-CINES8030494>.
 41. Cook, I.F., Barr, I., Hartel, G., Pond, D., and Hampson, A.W. (2006). Reactogenicity and immunogenicity of an inactivated influenza vaccine administered by intramuscular or subcutaneous injection in elderly adults. *Vaccine* 24, 2395–2402. <https://doi.org/10.1016/J.VACCINE.2005.11.057>.
 42. Prabhakaran, P., Gan, J., Feng, Y., Zhu, Z., Choudhry, V., Xiao, X., Ji, X., and Dimitrov, D.S. (2006). Structure of severe acute respiratory syndrome coronavirus receptor-binding domain complexed with neutralizing antibody. *J. Biol. Chem.* 281, 15829–15836. <https://doi.org/10.1074/JBC.M600697200>.
 43. Hwang, W.C., Lin, Y., Santelli, E., Sui, J., Jaroszewski, L., Stec, B., Farzan, M., Marasco, W.A., and Liddington, R.C. (2006). Structural basis of neutralization by a human anti-severe acute respiratory syndrome spike protein antibody. *J. Biol. Chem.* 281, 34610–34616. <https://doi.org/10.1074/JBC.M603275200>.
 44. Keler, T., He, L., Ramakrishna, V., and Champion, B. (2007). Antibody-targeted vaccines. *Oncogene* 26, 3758–3767. <https://doi.org/10.1038/sj.onc.1210375>.
 45. Braathen, R., Spång, H.C.L., Lindeberg, M.M., Fossum, E., Grødeland, G., Fredriksen, A.B., Bogen, B., and Jebsen, K.G. (2018). The magnitude and IgG subclass of antibodies elicited by targeted DNA vaccines are influenced by specificity for APC surface molecules. *ImmunoHorizons* 2, 38–53. <https://doi.org/10.4049/IMMUNOHORIZONS.1700038>.

46. Grodeland, G., Fredriksen, A.B., Løset, G.Å., Vikse, E., Fugger, L., and Bogen, B. (2016). Antigen targeting to human HLA class II molecules increases efficacy of DNA vaccination. *J. Immunol.* *197*, 3575–3585. <https://doi.org/10.4049/JIMMUNOL.1600893>.
47. Carayanniotis, G., and Barber, B.H. (1990). Characterization of the adjuvant-free serological response to protein antigens coupled to antibodies specific for class II MHC determinants. *Vaccine* *8*, 137–144. [https://doi.org/10.1016/0264-410X\(90\)90136-A](https://doi.org/10.1016/0264-410X(90)90136-A).
48. Snider, D.P., and Segal, D.M. (1987). Targeted antigen presentation using crosslinked antibody heteroaggregates. *J. Immunol.* *139*, 1609–1616.
49. Snider, D.P., Kaubisch, A., and Segal, D.M. (1990). Enhanced antigen immunogenicity induced by bispecific antibodies. *J. Exp. Med.* *171*, 1957–1963. <https://doi.org/10.1084/JEM.171.6.1957>.
50. Mao, T., Israelow, B., Peña-Hernández, M.A., Suberi, A., Zhou, L., Luyten, S., Reschke, M., Dong, H., Homer, R.J., Saltzman, W.M., and Iwasaki, A. (2022). Unadjuvanted intranasal spike vaccine elicits protective mucosal immunity against sarbecoviruses. *Science* *378*, eabo2523. <https://doi.org/10.1126/SCIENCE.ABO2523>.
51. Liu, X., Drelich, A., Li, W., Chen, C., Sun, Z., Shi, M., Adams, C., Mellors, J.W., Tseng, C.T., and Dimitrov, D.S. (2020). Enhanced elicitation of potent neutralizing antibodies by the SARS-CoV-2 spike receptor binding domain Fc fusion protein in mice. *Vaccine* *38*, 7205–7212. <https://doi.org/10.1016/J.VACCINE.2020.09.058>.
52. Cohen, A.A., Gnanaprasadam, P.N.P., Lee, Y.E., Hoffman, P.R., Ou, S., Kakutani, L.M., Keeffe, J.R., Wu, H.J., Howarth, M., West, A.P., et al. (2021). Mosaic nanoparticles elicit cross-reactive immune responses to zoonotic coronaviruses in mice. *Science* *371*, 735–741. <https://doi.org/10.1126/science.abf6840>.
53. Cohen, A.A., van Doremalen, N., Greaney, A.J., Andersen, H., Sharma, A., Starr, T.N., Keeffe, J.R., Fan, C., Schulz, J.E., Gnanaprasadam, P.N.P., et al. (2022). Mosaic RBD nanoparticles protect against challenge by diverse sarbecoviruses in animal models. *Science* *377*, eabq0839. <https://doi.org/10.1126/SCIENCE.ABQ0839>.
54. Sun, W., He, L., Zhang, H., Tian, X., Bai, Z., Sun, L., Yang, L., Jia, X., Bi, Y., Luo, T., et al. (2021). The self-assembled nanoparticle-based trimeric RBD mRNA vaccine elicits robust and durable protective immunity against SARS-CoV-2 in mice. *Signal Transduct. Target. Ther.* *6*, 340–411. <https://doi.org/10.1038/s41392-021-00750-w>.
55. Wang, W., Huang, B., Zhu, Y., Tan, W., and Zhu, M. (2021). Ferritin nanoparticle-based SARS-CoV-2 RBD vaccine induces a persistent antibody response and long-term memory in mice. *Cell. Mol. Immunol.* *18*, 749–751. <https://doi.org/10.1038/S41423-021-00643-6>.
56. Chen, R., Zhang, X., Yuan, Y., Deng, X., Wu, B., Xi, Z., Wang, G., Lin, Y., Li, R., Wang, X., et al. (2022). Development of receptor binding domain (RBD)-conjugated nanoparticle vaccines with broad neutralization against SARS-CoV-2 delta and other variants. *Adv. Sci.* *9*, e2105378. <https://doi.org/10.1002/ADVS.202105378>.
57. Lainsček, D., Fink, T., Forstnerič, V., Hafner-Bratkovič, I., Orehek, S., Strmšek, Ž., Manček-Keber, M., Pečan, P., Esih, H., Malenšek, Š., et al. (2021). A nanoscaffolded spike-rbd vaccine provides protection against sars-cov-2 with minimal anti-scaffold response. *Vaccines* *9*. <https://doi.org/10.3390/VACCINES9050431/S1>.
58. Ma, X., Zou, F., Yu, F., Li, R., Yuan, Y., Zhang, Y., Zhang, X., Deng, J., Chen, T., Song, Z., et al. (2020). Nanoparticle vaccines based on the receptor binding domain and heptad repeat (HR) of SARS-CoV-2 elicit robust protective immune responses. *Immunity* *53*, 1315–1330.e9. <https://doi.org/10.1016/J.IMMUNI.2020.11.015>.
59. Domenech de Cellès, M., Rohani, P., and King, A.A. (2019). Duration of immunity and effectiveness of Diphtheria-Tetanus-Acellular Pertussis vaccines in children. *JAMA Pediatr.* *173*, 588–594. <https://doi.org/10.1001/jamapediatrics.2019.0711>.
60. Hammarlund, E., Thomas, A., Poore, E.A., Amanna, I.J., Rynko, A.E., Mori, M., Chen, Z., and Slifka, M.K. (2016). Durability of vaccine-induced immunity against Tetanus and Diphtheria toxins: a cross-sectional analysis. *Clin. Infect. Dis.* *62*, 1111–1118. <https://doi.org/10.1093/CID/CIW066>.
61. World Health Organization. Electronic address: sageexecsec@who.int (2018). Tetanus vaccines: WHO position paper, February 2017 - Recommendations (2018). *Vaccine* *36*, 3573–3575. <https://doi.org/10.1016/J.VACCINE.2017.02.034>.
62. Bruel, T., Hadjadj, J., Maes, P., Planas, D., Seve, A., Staropoli, I., Guivel-Benhassine, F., Porrot, F., Bolland, W.H., Nguyen, Y., et al. (2022). Serum neutralization of SARS-CoV-2 Omicron sublineages BA.1 and BA.2 in patients receiving monoclonal antibodies. *Nat. Med.* *28*, 1297–1302. <https://doi.org/10.1038/s41591-022-01792-5>.
63. Iketani, S., Liu, L., Guo, Y., Liu, L., Chan, J.F.W., Huang, Y., Wang, M., Luo, Y., Yu, J., Chu, H., et al. (2022). Antibody evasion properties of SARS-CoV-2 Omicron sublineages. *Nature* *604*, 553–556. <https://doi.org/10.1038/s41586-022-04594-4>.
64. Takashita, E., Kinoshita, N., Yamayoshi, S., Sakai-Tagawa, Y., Fujisaki, S., Ito, M., Iwatsuki-Horimoto, K., Halfmann, P., Watanabe, S., Maeda, K., et al. (2022). Efficacy of antiviral agents against the SARS-CoV-2 Omicron subvariant BA.2. *N. Engl. J. Med.* *386*, 1475–1477. <https://doi.org/10.1056/NEJMc2201933>.
65. Desingu, P.A., and Nagarajan, K. (2022). The emergence of Omicron lineages BA.4 and BA.5, and the global spreading trend. *J. Med. Virol.* *94*, 5077–5079. <https://doi.org/10.1002/JMV.27967>.
66. Mykytyn, A.Z., Rissmann, M., Kok, A., Rosu, M.E., Schipper, D., Breugem, T.I., van den Doel, P.B., Chandler, F., Bestebroer, T., de Wit, M., et al. (2022). Antigenic cartography of SARS-CoV-2 reveals that Omicron BA.1 and BA.2 are antigenically distinct. *Sci. Immunol.* *7*, eabq4450. <https://doi.org/10.1126/SCIIMMUNOL.ABQ4450>.
67. Xia, H., Zou, J., Kurhade, C., Cai, H., Yang, Q., Cutler, M., Cooper, D., Muik, A., Jansen, K.U., Xie, X., et al. (2022). Neutralization of Omicron SARS-CoV-2 by 2 or 3 doses of BNT162b2 vaccine. Preprint at bioRxiv. <https://doi.org/10.1101/2022.01.21.476344>.
68. Muik, A., Lui, B.G., Wallisch, A.K., Bacher, M., Mühl, J., Reinholz, J., Ozhelvacı, O., Beckmann, N., Güimil Garcia, R.d.I.C., Poran, A., et al. (2022). Neutralization of SARS-CoV-2 Omicron by BNT162b2 mRNA vaccine-elicited human sera. *Science* *375*, 678–680. <https://doi.org/10.1126/SCIENCE.ABN7591>.
69. Evans, J.P., Zeng, C., Qu, P., Faraone, J., Zheng, Y.M., Carlin, C., Bednash, J.S., Zhou, T., Lozanski, G., Mallampalli, R., et al. (2022). Neutralization of SARS-CoV-2 Omicron sub-lineages BA.1, BA.1.1, and BA.2. *Cell Host Microbe* *30*, 1093–1102.e3. <https://doi.org/10.1016/J.CHOM.2022.04.014>.
70. Rujas, E., Kucharska, I., Tan, Y.Z., Benlekbir, S., Cui, H., Zhao, T., Wasney, G.A., Budyłowski, P., Guven, F., Newton, J.C., et al. (2021). Multivalency transforms SARS-CoV-2 antibodies into ultrapotent neutralizers. *Nat. Commun.* *12*, 3661–3712. <https://doi.org/10.1038/s41467-021-23825-2>.
71. Scheres, S.H.W. (2012). RELION: Implementation of a Bayesian approach to cryo-EM structure determination. *J. Struct. Biol.* *180*, 519–530. <https://doi.org/10.1016/J.JSB.2012.09.006>.
72. Morin, A., Eisenbraun, B., Key, J., Sanschagrin, P.C., Timony, M.A., Ottaviano, M., and Sliz, P. (2013). Collaboration gets the most out of software. *Elife*. <https://doi.org/10.7554/ELIFE.01456>.
73. Adams, P.D., Afonine, P.V., Bunkóczi, G., Chen, V.B., Davis, I.W., Echols, N., Headd, J.J., Hung, L.W., Kapral, G.J., Grosse-Kunstleve, R.W., et al. (2010). PHENIX: a comprehensive Python-based system for macromolecular structure solution. *Acta Crystallogr. D Biol. Crystallogr.* *66*, 213–221. <https://doi.org/10.1107/S0907444909052925>.
74. Kabsch, W. (2010). Xds. *Acta Crystallogr. D Biol. Crystallogr.* *66*, 125–132. <https://doi.org/10.1107/S0907444909047337>.
75. Emsley, P., Lohkamp, B., Scott, W.G., and Cowtan, K. (2010). Features and development of Coot. *Acta Crystallogr. D Biol. Crystallogr.* *66*, 486–501. <https://doi.org/10.1107/S0907444910007493>.

76. Booth, D.S., Avila-Sakar, A., and Cheng, Y. (2011). Visualizing proteins and macromolecular complexes by negative stain EM: from grid preparation to image acquisition. *J. Vis. Exp.* <https://doi.org/10.3791/3227>.
77. Menezes, J., Leibold, W., Klein, G., and Clements, G. (1975). Establishment and characterization of an Epstein-Barr virus (EBV)-negative lymphoblastoid B cell line (BJA-B) from an exceptional, EBV-genome-negative African Burkitt's lymphoma. *Biomedicine* *22*, 276–284.
78. Scally, S.W., Petersen, J., Law, S.C., Dudek, N.L., Nel, H.J., Loh, K.L., Wijeyewickrema, L.C., Eckle, S.B.G., van Heemst, J., Pike, R.N., et al. (2013). A molecular basis for the association of the HLA-DRB1 locus, citrullination, and rheumatoid arthritis. *J. Exp. Med.* *210*, 2569–2582. <https://doi.org/10.1084/JEM.20131241>.
79. McCoy, A.J., Grosse-Kunstleve, R.W., Adams, P.D., Winn, M.D., Storoni, L.C., and Read, R.J. (2007). Phaser crystallographic software. *J. Appl. Crystallogr.* *40*, 658–674. <https://doi.org/10.1107/S0021889807021206>.
80. Corman, V.M., Landt, O., Kaiser, M., Molenkamp, R., Meijer, A., Chu, D.K., Bleicker, T., Brünink, S., Schneider, J., Schmidt, M.L., et al. (2020). Detection of 2019 novel coronavirus (2019-nCoV) by real-time RT-PCR. *Euro Surveill.* *25*, 2000045. <https://doi.org/10.2807/1560-7917.ES.2020.25.3.2000045>.

STAR★METHODS

KEY RESOURCES TABLE

REAGENT or RESOURCE	SOURCE	IDENTIFIER
Antibodies		
Alexa Fluor® 488 AffiniPure Goat Anti-Human IgG, Fc γ fragment specific	Jackson ImmunoResearch	Cat#109-545-098; RRID: AB_2337840
Goat Anti-Rabbit IgG H&L (HRP)	Abcam	Cat#ab97051; RRID: AB_10679369
Goat Anti-Ferret IgG H&L (HRP)	Abcam	Cat#ab112770 RRID: AB_10862402
Bacterial and virus strains		
SARS-CoV-2 (hCoV-19/Canada/ON-VIDO-01/2020)	Vaccine and Infectious Disease Organization (VIDO)	N/A
Biological samples		
Human PBMCs	Canadian Blood Services (CBS)	N/A
Chemicals, peptides, and recombinant proteins		
SARS-CoV-2 spike protein RBD	Florian Krammer, Icahn School of Medicine at Mount Sinai	N/A
SARS-CoV Spike/RBD Protein (RBD, His Tag)	Sino Biological	Cat#40150-V08B2
Human ACE2 (hACE2)	Rujas et al. ⁷⁰	N/A
c44H10 IgG	This paper	N/A
c44H10 Fab	This paper	N/A
ITV	This paper	N/A
ITV-TpD	This paper	N/A
ITV-PADRE	This paper	N/A
ITV-TpD (Bi-Antigenic)	This paper	N/A
HLA-DR (A*01:01 / B1*04:01)	This paper	N/A
HLA-DR (A*01:01+W168R / B1*04:01)	This paper	N/A
HLA-DR (A*01:01 / B1*04:01+F31I/H33N)	This paper	N/A
HLA-DR (A*01:01 / B1*04:01+F31V/H33N)	This paper	N/A
HLA-DR (A*01:01+W168R / B1*04:01+F31I/H33N)	This paper	N/A
HLA-DR (A*01:01+W168R / B1*04:01+F31V/H33N)	This paper	N/A
SARS-CoV-2 Spike protein (RBD, Avi & His Tag)-HRP	Genscript	Cat#Z03594
GIBCO™ FreeStyle™ 293 Expression Medium	Thermo Fisher Scientific	Cat#12338026
FectoPRO DNA Transfection Reagent	VWR	Cat#10118-444
BioT transfection reagent	Bioland Scientific	Cat#B01-01
britelite plus Reporter Gene Assay System	Perkin Elmer	Cat#6066769
Td ADSORBED	Sanofi Pasteur, VaccineShoppeCanada	Cat#482229
Alhydrogel® (alum) adjuvant 2%	Invivogen	Cat#vac-alu-50
Alexa Fluor™ 488 C ₅ Maleimide	Thermo Fisher Scientific	Cat#A10254
TriPure™ Isolation Reagent	Sigma Aldrich	Cat#11667157001
Uranyl Formate	Thermo Fisher Scientific	Cat#50-189-8757
Critical commercial assays		
Octet® Protein A (ProA) Biosensors	Sartorius	Cat#18-5010
Octet® Anti-Penta-HIS (HIS1K) Biosensors	Sartorius	Cat#18-5120
4X TaqMan Fast Virus one step RT-PCR kit	Thermo Fisher Scientific	Cat# 4444434
gBlock	Integrated DNA Technologies	Custom

(Continued on next page)

Continued

REAGENT or RESOURCE	SOURCE	IDENTIFIER
Deposited data		
Crystal structure of c44H10 Fab-MHC class II complex	This paper	PDB: 8EUQ
Experimental models: Cell lines		
FreeStyle™ 293-F Cells	Thermo Fisher Scientific	Cat#R79007
Expi293F GnTI ^{-/-} Cells	Thermo Fisher Scientific	Cat#A39240
BJAB Cells	DSMZ	Cat#ACC757
HEK293T Cells	ATCC	Cat#CRL-3216
HEK293T-ACE2 Cells	BEI Resources	Cat#NR52511
Vero E6 Cells	ATCC	Cat#CRL-1586
Experimental models: Organisms/strains		
New Zealand White Rabbits	Cedarlane Laboratories	N/A
European Ferrets	Marshall Bioresources	N/A
Recombinant DNA		
pCAGGS-SARS-CoV-2-RBD_His	Florian Krammer, Icahn School of Medicine at Mount Sinai	N/A
pcDNA3.4-hACE2_His	Rujas et al. ⁷⁰	N/A
pcDNA3.4-ITV-HC-CoV2RBD	This paper	N/A
pcDNA3.4-ITV-KC	This paper	N/A
pcDNA3.4-ITV-KC-TpD	This paper	N/A
pcDNA3.4-ITV-KC-PADRE	This paper	N/A
pcDNA3.4-ITV-KC-CoV1RBD-TpD	This paper	N/A
pcDNA3.4-HLA-DR-A*01:01_His	This paper	N/A
pcDNA3.4-HLA-DR-A*01:01-W168R_His	This paper	N/A
pcDNA3.4-HLA-DR-B*04:01_His	This paper	N/A
pcDNA3.4-HLA-DR-B*04:01- F31I/H33N_His	This paper	N/A
pcDNA3.4-HLA-DR-B*04:01- F31V/H33N_His	This paper	N/A
pcDNA3.4-REGN10933-IgG-HC	Hansen et al. ³¹	N/A
pcDNA3.4-REGN10933-KC	Hansen et al. ³¹	N/A
pcDNA3.4-REGN10987-IgG-HC	Hansen et al. ³¹	N/A
pcDNA3.4-REGN10987-KC	Hansen et al. ³¹	N/A
pcDNA3.4-COV2-2196-IgG-HC	Zost et al. ³⁰	N/A
pcDNA3.4-COV2-2196-KC	Zost et al. ³⁰	N/A
pcDNA3.4-CR3022-IgG-HC	Yuan et al. ²⁹	N/A
pcDNA3.4-CR3022-KC	Yuan et al. ²⁹	N/A
pcDNA3.4-m396-IgG-HC	Prabakaran et al. ⁴²	N/A
pcDNA3.4-m396-KC	Prabakaran et al. ⁴²	N/A
pcDNA3.4-80R-IgG-HC	Hwang et al. ⁴³	N/A
pcDNA3.4-80R-KC	Hwang et al. ⁴³	N/A
pCAGGS-SARS-CoV-2-Wuhan-Hu-1 Spike Glycoprotein Gene	BEI Resources	Cat#NR52310
Lentiviral backbone with Luc2; ZsGreen insert	BEI Resources	Cat#NR52516
Helper plasmid with Tat1b insert	BEI Resources	Cat#NR52518
Helper plasmid with Gag; pol insert	BEI Resources	Cat#NR52517
Helper plasmid with Rev1b insert	BEI Resources	Cat#NR52519
SARS-CoV-2-Wuhan-Hu-1 Spike Glycoprotein Gene, Beta variant	David Ho, Columbia University	N/A
SARS-CoV-2-Wuhan-Hu-1 Spike Glycoprotein Gene, Gamma variant	David Ho, Columbia University	N/A

(Continued on next page)

Continued

REAGENT or RESOURCE	SOURCE	IDENTIFIER
SARS-CoV-2-Wuhan-Hu-1 Spike Glycoprotein Gene, Delta variant	David Ho, Columbia University	N/A
SARS-CoV-2-Wuhan-Hu-1 Spike Glycoprotein Gene, Omicron BA.1 variant	Dennis Burton, Scripps Research Institute	N/A
SARS-CoV-2-Wuhan-Hu-1 Spike Glycoprotein Gene, Omicron BA.5 variant	GISAID	Accession #EPI_ISL_11542604
Software and algorithms		
Relion	Scheres ⁷¹	https://relion.readthedocs.io/en/release-3.1/Installation.html
FlowJo	FlowJo, LLC	https://www.flowjo.com/solutions/flowjo/downloads
SBGrid	Morin et al. ⁷²	https://sbgrid.org/software/titles/sbgrid-installer
Phenix	Adams et al. ⁷³	http://www.phenix-online.org/
XDS	Kabsch ⁷⁴	https://xds.mr.mpg.de/html_doc/downloading.html
Coot	Emsley et al. ⁷⁵	https://www2.mrc-lmb.cam.ac.uk/personal/pemsley/cool/
PRISM Graphpad	GraphPad Software, LLC	https://www.graphpad.com/scientific-software/prism/
Other		
PDBePisa server	Krissinel and Henrick ³³	https://www.ebi.ac.uk/pdbe/pisa/
IPD-IMGT/HLA database	Robinson et al. ³⁴	https://www.ebi.ac.uk/ipd/imgt/hla/
Homemade carbon grids	Booth et al. ⁷⁶	N/A

RESOURCE AVAILABILITY

Lead contact

Further information and requests for resources and reagents should be directed to and will be fulfilled by the Lead Contact, Jean-Philippe Julien (jean-philippe.julien@sickkids.ca).

Materials availability

All unique and stable reagents generated in this study are available via the [lead contact](#) upon a reasonable request.

Data and code availability

- The crystal structure has been deposited to the Protein Data Bank and is publicly available as of the date of publication. Accession numbers are listed in the [key resources table](#).
- This paper does not report original code.
- Any additional information required to reanalyze the data reported in this paper is available from the [lead contact](#) upon request.

EXPERIMENTAL MODEL AND SUBJECT DETAILS

Mammalian cell lines and culture conditions

Female mammalian cells (FreeStyle™ 293-F cells, Thermo Fisher Scientific; HEK 293S, GnT I^{-/-} cells, ATCC) were cultured in suspension in GIBCO™ FreeStyle™ 293 Expression Medium (Thermo Fisher Scientific) at 37°C in a Multitron Pro Shaker (Infors HT) with 70% humidity, 8% CO₂ and rotating at 130 rpm. B lymphoblastoid BJAB cells (DSMZ)⁷⁷ were grown in RPMI medium supplemented with 10% fetal bovine serum (FBS) and 1% penicillin/streptomycin (all from Thermo Scientific) in a 37°C, 5% CO₂ incubator. For pseudovirus neutralization assays, HEK293T cells (ATCC) and HEK293T-ACE2 cells (BEI NR52511) were cultured in DMEM media supplemented with 10% heat-inactivated FBS (Gibco), 2.5% HEPES (Gibco) and 0.5% gentamicin (ThermoFisher) in a 37°C, 5% CO₂ incubator. Vero E6 cells (ATCC) were maintained in a humidified incubator at 37°C, 5% CO₂ in DMEM (Corning) supplemented with 10% FBS.

Rabbits

New Zealand White Rabbits were bred internally and housed individually or in pairs at Cedarlane Laboratories' registered facility (Burlington, Ontario, Canada). Immunization studies were conducted on female rabbits aged approximately 3 months. All procedures were conducted in accordance with Cedarlane's Animal Care Committee and standard operating protocols were reviewed and approved by the facility's governing body.

Ferrets

European ferrets (*Mustela furo*) were ordered from Marshall Farms (New York) and transported to the Canadian Science Centre for Human and Animal Health (CSCHAH) in a climate-controlled vehicle. Each experimental group was composed of 3 male and 3 female ferrets aged approximately 6 months. On arrival, the animals were housed in caging units in the BSL3 Ag facility at the Canadian Food Inspection Agency – National Centre for Foreign Animal Disease (CFIA-NCFAD). Animals were acclimatized for 7 days prior to the start of the experiment and were checked daily by trained animal care staff. Animals were observed during acclimation, convalescence and all stages of infection. Ferret experiments were conducted under the approval of the CSCHAH Animal Care Committee which follows the guidelines of the Canadian Council on Animal Care.

Human PBMCs

PBMC samples were from healthy donors provided as EDTA whole blood by the Canadian Blood Services. All donors provided informed consent of use of donations for research purposes prior to donation.

METHOD DETAILS

Plasmid design and synthesis

DNA plasmids for the expression of all proteins described in this work were designed in the pcDNA3.4 TOPO mammalian expression vector and optimized for *Homo sapiens* expression at GeneArt (Invitrogen). These constructs were maxiprep using PureLink HiPure Plasmid Maxiprep Kits (Invitrogen).

Expression and purification of recombinant ITVs and anti-RBD mAbs

FreeStyle 293-F cells were split to a density of 0.8×10^6 cells/mL at least one hour before transfection. Cells were transfected using FectoPRO Reagent (Polyplus) following manufacturer instructions at a 1:1 DNA to FectoPRO ratio. 90 μ g of plasmid DNA was used for transfection (2:1 ratio of heavy and light chain DNA plasmids) for every 200 mL of cell culture. Transfected cells were incubated in a 37°C, 5% CO₂ shaking incubator for 5 to 7 days to allow for the expression and pairing of heavy and light chain gene products. Transfected cell culture supernatants were collected and filtered through 0.22 μ m Steritop filters (Millipore Sigma) before loading onto protein A affinity columns using the ÄKTA start protein purification system (Cytiva Life Sciences). Following loading, samples were washed with 1X phosphate-buffered saline (PBS) then eluted with 100 mM glycine, pH 2.2 and immediately neutralized with 1 M Tris, pH 9.0. Elution fractions were concentrated using Amicon 30K Ultra-0.5 mL Centrifugal Filters (Millipore Sigma) and buffer-exchanged into PBS with PD-10 desalting columns (Cytiva). All purified proteins were validated for integrity and purity via sodium dodecyl sulfate polyacrylamide gel electrophoresis (SDS-PAGE) and stored at -80°C until use.

Expression and purification of recombinant c44H10 Fab

c44H10 Fab heavy and light chain plasmids were transfected into FreeStyle 293-F cells as described above. Recombinant c44H10 Fab was purified by KappaSelect affinity chromatography with 100 mM glycine, pH 2.2 elution and immediate 1 M Tris, pH 9.0 neutralization, followed by MonoS ion exchange chromatography using 20 mM NaOAc, pH 5.6 \pm 1M KCl, and size exclusion chromatography on a Superdex 200 Increase 10/300 GL in 20 mM Tris, pH 8.0, 150 mM NaCl (TBS) (Cytiva).

Expression and purification of recombinant SARS-CoV-2 RBD and hACE2

FreeStyle 293-F cells were transfected as described above with 50 μ g of plasmid DNA encoding the SARS-CoV-2 RBD or human ACE2 (hACE2) per 200 mL of cell culture. Recombinant proteins were purified by affinity chromatography via a HisTrap Ni-NTA column (Cytiva) and eluted using 20 mM Tris pH 8.0, 500 mM imidazole buffer. Subsequent size exclusion chromatography was performed in 20 mM Tris, pH 8.0, 150 mM NaCl on a Superdex 200 Increase column (Cytiva).

Design, expression and purification of recombinant MHC Class II

The extracellular domains of MHC Class II (DRA*01:01/DRB1*04:01) α and β chains were designed in pcDNA3.4 TOPO, with both chains containing C-terminal Tobacco Etch Virus (TEV)-cleavable Fos/Jun zippers to promote dimerization and 6xHis tags for purification purposes.⁷⁸ The MHC Class II molecule was expressed with the Influenza Hemagglutinin (HA) peptide covalently attached via a flexible linker to the N terminus of the β chain to promote proper folding of the α/β dimer. HLA-DR α and β chain plasmids were co-transfected in a 1:1 ratio (50 μ g total per 200 mL of cell culture) into HEK 293S (GnT1^{-/-}) cells. Recombinant MHC Class II was purified by affinity chromatography via a HisTrap Ni-NTA column (Cytiva) and eluted using 20 mM Tris, pH 8.0, 500 mM imidazole. Subsequent size exclusion chromatography was performed in TBS, pH 8.0 on a Superdex 200 Increase 10/300 GL (Cytiva). Purified

MHC Class II was subjected to overnight treatment with EndoH and TEV proteases at ratios of 5:1 and 20:1, respectively, for deglycosylation and cleavage of the Fos/Jun zipper. A second round of affinity and size exclusion purifications was performed on cleaved MHC Class II before complexation with c44H10 Fab for crystallization trials.

Dynamic Light Scattering of RBD, c44H10 IgG and ITV

Dynamic light scattering (DLS) analysis was performed using a DynaPro Plate Reader III (Wyatt Technology). 20 μ L of each protein at 1 mg/mL were added to a 384-well black, clear bottom plate (Corning) and measured at a fixed temperature of 25 $^{\circ}$ C with a duration of 5 s per read. Particle hydrodynamic radii (Rh) and polydispersity (% Pd) were obtained from the accumulation of ten reads from duplicate samples using the Dynamics software (Wyatt Technology).

Negative-stain electron microscopy

Purified ITV protein was diluted to 20 μ g/mL, applied onto homemade carbon film-coated grids⁷⁶ (previously glow-discharged in air for 15 s) and stained with 2% uranyl formate. Grids were imaged with a Hitachi HT7800 TEM operating at 120 kV, with a calibrated pixel size of 1.83 \AA /pix. Particle selection, extraction and 2D classification were performed with Relion 3.1.⁷¹

Fluorescent labeling of anti-RBD mAbs for flow cytometry

Purified anti-RBD mAbs were diluted to 100 μ M in PBS and incubated in a 10-fold molar excess of TCEP at room temperature for 30 min. Alexa Fluor 488 (AF488) C₅ Maleimide dye (Invitrogen) was added to each reaction at a concentration of 10 mM. Samples were incubated overnight at 4 $^{\circ}$ C protected from light. Free, unconjugated dye was washed out of solution using PBS and Amicon 30K Ultra-0.5 mL Centrifugal Filters (Millipore Sigma). The concentration of labeled protein was assessed by Nanodrop measurement at 280 nm.

Flow cytometry for confirmation of MHC class II-targeting and RBD structural integrity

BJAB cells were collected in a conical tube and centrifuged at 300 g for 5 min. Cell pellets were resuspended in staining buffer (PBS, 2% FBS, 0.05% NaN₃) at 1×10^6 cells/mL, and 200 μ L of the cell suspension was dispensed into the wells of a polystyrene, V-bottom 96-well plate (Greiner Bio-One) for staining. Cells were centrifuged at 300 g for 5 min, and then incubated in Fc Block (BD Biosciences) for 10 min at room temperature. Purified ITV was then added to the cells at 10 μ g/mL and left to incubate for 1 h at 4 $^{\circ}$ C. For the confirmation of ITV binding to MHC Class II, cells were washed twice, then stained with AF488 AffiniPure Goat Anti-Human IgG, Fc γ fragment specific (1:1,000, Jackson ImmunoResearch) for 30 min at 4 $^{\circ}$ C. For the probing of RBD structural integrity, AF488 pre-labeled anti-RBD mAbs (REGN10987, REGN10933, m396, 80R) were used as secondary at 10 μ g/mL in lieu of anti-IgG secondary. After two additional washes, cells were resuspended in propidium iodide (1:100, Thermo Scientific) for the exclusion of dead cells and debris. An isotype-matched antibody served as a negative control. Samples were acquired on BD LSR II or LSR Fortessa cell analyzers using the BD FACSDivaTM Software, and further analyzed using the FlowJoTM Software.

Flow cytometry for 44H10 binding to human PBMCs

Peripheral blood mononuclear cells (PBMC) cells were isolated by density centrifugation using Ficoll-Hypaque solution (GE Healthcare). PBMC were resuspended in staining buffer (PBS, 2% FCS, 1mM EDTA) and Fc receptors were blocked with Human TruStain FcXTM (Biolegend) according to the manufacturer's instructions. PBMCs were then stained for 1 h at 4 $^{\circ}$ C with 50 μ L of 0.1 mg/mL AF488 pre-labeled c44H10 IgG. AF488-conjugated Human IgG1 was used as isotype control. Samples were acquired on a Sony SP6800 Spectral Analyzer and processed using the FlowJoTM Software.

Bi-layer interferometry for measurement of recombinant MHC class II-c44H10/ITV binding

Real-time analysis of binding kinetics was measured using the Octet RED96 BLI system (Sartorius). Baseline, association, and dissociation steps were conducted at 25 $^{\circ}$ C for 180 s in kinetics buffer (PBS, pH 7.4, 0.01% BSA, 0.002% Tween). Recombinant MHC Class II was loaded onto Penta-His Biosensors (FortéBio) at 10 μ g/mL until a threshold response of 0.7 nm. Association events were measured by dipping loaded biosensors into wells containing a two-fold serial dilution of c44H10 IgG or ITV at a 250 nM starting concentration. Dissociation was measured by transfer of biosensors back into buffer-containing wells. Biosensors were regenerated in 10 mM glycine, pH 1.5. Kinetics data were analyzed using the FortéBio Octet Data Analysis software 9.0.0.6, and curves were fitted to a 1:1 binding model for calculation of K_D , K_{on} and K_{off} .

Bi-layer interferometry for measurement of ITV binding to hACE2

Purified ITV was loaded onto Protein A biosensors (FortéBio) at 10 μ g/mL until a threshold response of 0.7 nm, and association events were measured by dipping loaded biosensors into wells containing a two-fold serial dilution of hACE2 at a 500 nM starting concentration. Dissociation was measured by transfer of biosensors back into buffer-containing wells. Biosensors were regenerated in 100 mM glycine, pH 2.2. Kinetics data were analyzed using the FortéBio Octet Data Analysis software 9.0.0.6, and curves were fitted to a 1:1 binding model for calculation of K_D , K_{on} and K_{off} .

Co-crystallization and structure determination of the c44H10 Fab-MHC class II complex

c44H10 Fab was mixed with recombinant MHC Class II in a 1.5-molar excess, and excess Fab was purified away via size exclusion chromatography (Superdex 200 Increase 10/300 GL, Cytiva). The protein complex was concentrated to 8 mg/mL and mixed with a mother liquor of 1.7 M ammonium sulfate, 15% glycerol, 0.085 M HEPES, 1.7% PEG400, as well as crystal seeds previously obtained in a condition of 2 M ammonium sulfate and 0.1 M bis-tris pH 5.5, in a ratio of 2:1:3 (protein:seed:mother liquor). Crystals appeared after ~120 days and grew steadily until day ~160, at which time they were cryoprotected in 15% (v/v) ethylene glycol before being flash-frozen in liquid nitrogen. Data were collected at the 23-ID-D beamline at the Argonne National Laboratory Advanced Photon Source. Datasets were processed, merged and scaled using XDS and Xprep.⁷⁴ The structure was determined by molecular replacement using Phaser.⁷⁹ Refinement of the structure was performed using phenix.refine⁷³ and Coot.⁷⁵ Access to all software was supported through SGrid.⁷² Sequences of known HLA-DRA and HLA-DRB1 alleles were aligned using the IPD-IMGT/HLA database sequence alignment tool,³⁴ and interactions were analyzed using the PDBePisa server.³³

Endotoxin measurements and removal for *in vivo* studies

Endotoxin levels in RBD, ITV, ITV-TpD or ITV-PADRE protein samples were measured using the EndoSafe Nexgen-PTS System (Charles River). The threshold for samples suitable for immunization was < 5 EU/mL. When required, endotoxin removal was performed using a ToxinEraser endotoxin removal kit (GenScript) per the manufacturer's instructions and retested until endotoxin levels measured were below the threshold value.

Rabbit immunizations

Female New Zealand white rabbits housed at Cedarlane Laboratories were immunized at day 0 via SQ or IM injection with unadjuvanted RBD, ITV, ITV-TpD or ITV-PADRE, followed by a boost at day 35. For the study assessing the role of existing anti-TD immunity in ITV-TpD immunogenicity, rabbits were intramuscularly immunized 28 days before the ITV/ITV-TpD prime with ¼ of the human dose of Td Adsorbed vaccine (Sanofi®), or PBS. For serum preparation, blood was collected into red top vacutainer tubes and incubated at 3-4 h at room temperature to allow for clotting. The tubes were centrifuged at 4 °C at 3000 rpm for 20 min, and supernatants were poured off into appropriate tubes and stored at -20°C before shipping on dry ice.

ELISA measurement of anti-RBD titers elicited in rabbits

Immulon 4 HBX ELISA plates (Thermo Scientific) were coated overnight at 4°C with 100 ng/well SARS-CoV-2 spike RBD (produced in-house) or SARS-CoV-1 spike RBD (Sino Biological). All subsequent steps were conducted at room temperature. Plates were washed three times with PBS-T (PBS, 0.1% Tween), then incubated with blocking buffer (PBS-T, 3% non-fat milk) for 1 h. The blocking solution was discarded and 100 µL of rabbit sera pre-diluted in diluent buffer (PBS-T, 1% milk) and standard (rabbit anti-SARS-CoV-2 spike RBD polyclonal antibody, Cedarlane) were added to the ELISA plates. After a 2 h incubation, plates were washed three times with PBS-T and incubated with Goat Anti-Rabbit IgG H&L (HRP) secondary antibody (1:10,000, Abcam) for 1 h. Plates were once more washed three times, then developed using a TMB Substrate Reagent Set (BD) following manufacturer instructions; reactions were stopped at 5 min by the addition of 2 N HCl. Absorbance readings at 450 nm were acquired using a Synergy Neo2 Multi-Mode Assay Microplate Reader (Biotek Instruments). Data were plotted in Prism v9.3.1 (GraphPad) and antibody concentration was extrapolated from absorbance using four-parameter logistic (4PL) regression of log-transformed values.

ELISA measurement of antibody avidity index

ELISAs were performed as described above, with an added 15 min incubation with 1.5 M NaSCN following the primary incubation with rabbit serum. Avidity index was defined as the percentage of antibodies in serum that remain bound to the RBD-coated plate after chaotrope treatment, and was calculated using the following formula:

$$\text{Avidity Index} = \frac{\text{Titer with 1.5 M NaSCN treatment}}{\text{Titer without NaSCN treatment}} \times 100\%$$

Surrogate virus neutralization assay (sVNT)

Immulon 4 HBX ELISA plates (Thermo Scientific) were coated overnight at 4°C with 200 ng/well recombinant hACE2, followed by blocking with 3% BSA in PBS-T for 1 h at room temperature. To simulate viral neutralization, a 1:500 dilution of RBD-HRP (GenScript) was pre-incubated with serially diluted serum samples for 1 h at 37°C, subsequently added to blocked plates, and further incubated for 1 h at room temperature. Plates were washed three times with PBS-T prior to colorimetric development with TMB for 15 min. Absorbance data at 450 nm were converted to % inhibition using the following formula:

$$\% \text{ Inhibition} = \left[1 - \frac{(OD_{\text{sample}} - OD_{\text{min}})}{(OD_{\text{max}} - OD_{\text{min}})} \right] \times 100\%$$

Pseudovirus production

Pseudovirus production was conducted as previously described.⁷⁰ Briefly, 293T cells were co-transfected with a lentiviral backbone encoding the luciferase reporter gene (BEI NR52516), a plasmid expressing the SARS-CoV-2 Spike (BEI NR52310) and plasmids encoding the HIV structural and regulatory proteins Tat (BEI NR52518), Gag-pol (BEI NR52517) and Rev (BEI NR52519). Co-transfection of the five plasmids was performed using BioT reagent (Bioland Scientific) following manufacturer instructions. 24 h post-transfection at 37°C, the media was supplemented with 5 mM sodium butyrate (NaB) and the cells were incubated for an additional 24 h at 30°C prior to pseudovirus (PsV) harvesting. Beta (B.1.351), Gamma (P.1), and Delta (B.1.617.2) SARS-CoV-2 PsV variants were generated by substituting the wild-type spike plasmid with the respective VOC spike using plasmids kindly provided by David Ho (Columbia). Omicron (BA.1) variant PsV was generated using a spike plasmid kindly provided by Dennis Burton (The Scripps Research Institute), and Omicron (BA.5) variant PsV was generated using a spike plasmid synthesized at GeneArt (Invitrogen). PsV were harvested, filtered through 0.45 µm sterile filters, and concentrated using 100 K Amicon filters (Millipore Sigma).

Pseudovirus neutralization assay (pVNT)

Neutralization assays were performed using 293T-ACE2 cells (BEI NR52511) as previously described³⁸ with few modifications.⁷⁰ Briefly, rabbit sera were inactivated for 30 min at 56°C. Serial dilutions of the inactivated sera were incubated for 1 h at 37°C with SARS-CoV-2 PsV and subsequently added to 293T-ACE2 cells (BEI NR52511) seeded in Poly-L-lysine (Sigma-Aldrich) coated plates 24 h prior to the experiment. A final concentration of 5 µg/ml polybrene (Sigma-Aldrich) was added to the PsV-sera mixtures. After 48 h of incubation at 37°C, neutralization was monitored by adding 50 µl of Britelite plus reagent (PerkinElmer) to 50 µl of cells for 2 min. Supernatants were transferred to a 96-well white plate (Sigma-Aldrich) to measure luminescence in relative light units (RLUs) using a Synergy Neo2 Multi-Mode Assay Microplate Reader (Biotek Instruments). Absorbance data were converted to % inhibition using the same formula as used in the sVNT. Plotted data are the average of at least three replicate measurements. Data were fitted using 4PL regression constrained at top = 100% and bottom = 0% in GraphPad Prism 9.3.1 for determination of neutralization titers.

Ferret immunizations and challenge

Ferrets were immunized intramuscularly with 50 µg of unadjuvanted ITV-TpD or an RBD-equimolar dose of Alum-adjuvanted RBD on day 0 and day 35. Unvaccinated ferrets were immunized with an equal volume of sterile PBS. Each group of six animals consisted of three males and three females. SARS-CoV-2 (hCoV-19/Canada/ON-VIDO-01/2020) (VIDO) was grown and maintained in VeroE6 cells at CFIA-NCFAD Level 3 (Zoonotic). Ferrets were challenged on day 49 with 10⁶ pfu SARS-CoV-2 (Wuhan-Hu-1) intranasally (50 µL per nostril, 100 µL total). Blood samples were collected in BD serum-separator microtainer tubes (BD 365967) except on day 14 post-challenge, where blood was collected in 5 mL BD vacutainer serum-separator tubes (BD 367989) upon euthanasia. Serum separated from blood and nasal washes performed using 1 mL PBS were stored in 2 mL screw cap micro tubes (Sarstedt) at -80°C until use.

ELISA measurement of anti-RBD titers elicited in ferrets

96-well flat bottom plates (Nunc) (Thermo Scientific) were coated with 50 ng/well of RBD in 0.05 M carbonate-bicarbonate buffer (Sigma-Aldrich) overnight at 4°C. Plates were washed 5 times with 0.01 M PBS-T and blocked with 1X Casein Blocking Buffer (Sigma-Aldrich) for 1 h shaking at 37°C. Plates were washed and dilutions of serum samples were prepared in casein blocking buffer and incubated for 1 h shaking at 37°C. Plates were washed and incubated with goat anti-ferret IgG-HRP (1:10,000, Abcam) for 1 h shaking at 37°C. Plates were washed and developed with TMB (ThermoFisher Scientific) following manufacturer instructions; reactions were stopped by the addition of Stop Solution 0.16 M sulphuric acid (ThermoFisher Scientific). Absorbance of the plates was read at 450 nm.

Plaque reduction neutralization titer (PRNT) assay

Serum samples were heat-inactivated at 56°C for 30 min. Two-fold serial dilutions of inactivated sera were incubated with 100 pfu of SARS-CoV-2 virus for 1 h at 37°C. Each virus-serum mixture was then added to wells of > 90% confluent Vero E6 cells in a 48-well format, incubated for 1 h at 37°C in 5% CO₂, then overlaid with 500 µL of 2% carboxymethyl cellulose (Sigma) in supplemented DMEM (Corning) per well. Plates were incubated at 37°C for 72 h, fixed with 10% buffered formalin and stained with 0.5% crystal violet. Serum dilutions resulting in > 70% reduction of plaque counts compared to virus-only controls were considered positive for virus neutralization.

RNA extraction from nasal washes

Total RNA extraction from nasal washes was conducted using the MagMAX CORE Nucleic Acid Purification Kit (ThermoFisher) on the Thermo Scientific Kingfisher benchtop automated extraction instrument, using TriPure Isolation reagent (Sigma Aldrich) in a 1:9 v/v ratio instead of the kit-supplied Lysis Solution. 650 µL inactivated sample, 30 µL binding beads and 350 µL binding buffer spiked with Armoured RNA-Enterovirus (ARM-ENTERO, Asuragen) were then used for RNA extraction in 96 deep-well plates. Extracted RNA was recovered in 30 µL elution buffer. The spiked enteroviral armoured RNA was used as an exogenous RNA extraction control.

RT-qPCR for measurement of viral titers in nasal washes

RNA extracted from nasal washes was tested for the presence of SARS-CoV-2 RNA by an E gene RT-qPCR that detects a broad range of human and bat coronaviruses.⁸⁰ For the detection of SARS-CoV-2 RNA by RT-qPCR, 4X TaqMan Fast Virus one step RT-PCR kit (LifeTech) was used according to manufacturer's recommendations. For each RT-qPCR reaction, 0.4 μ M of E gene forward and reverse primers, 0.2 μ M of ARM-ENTERO forward and reverse primers and 0.2 μ M of both probes were used. RT-qPCR runs were performed using a 7500 Fast Real-Time PCR system (Applied Biosystems) using the following cycle conditions: 50°C for 5 min, 95°C for 20 s, then 40 cycles of 95°C for 3 s followed by 60°C for 30 s. RT-qPCR semi-quantitative results were calculated based on a gBlock (Integrated DNA Technologies) standard curve for SARS-CoV-2 E gene.

Virus isolation from nasal washes

To titrate live SARS-CoV-2 virus in the nasal washes of the ferrets, two-fold serial dilutions of nasal washes were added to wells of > 90% confluent Vero E6 cells in a 48-well format, incubated for 1 h at 37°C in 5% CO₂, then overlaid with 500 μ L of 2% carboxymethyl cellulose (Sigma) in supplemented DMEM (Corning) per well. Plates were incubated at 37°C for 72 h, fixed with 10% buffered formalin and stained with 0.5% crystal violet. Plaques were counted and the endpoint dilution was taken as the relative live-virus titres in the nasal washes.

QUANTIFICATION AND STATISTICAL ANALYSIS

All data and statistical analyses were performed using Prism v9.3.1 (GraphPad). Wherever applicable, the normality of the data was determined by Shapiro-Wilk test to select the most appropriate statistical test. For comparison of two groups, Student's-t test (normal distribution) or Mann-Whitney (abnormal distribution) were performed. For comparison of more than two groups, one-way ANOVA (normal distribution) or Kruskal-Wallis followed by Dunn's multiple comparisons test (abnormal distribution) were performed.